Aalto University
School of Engineering

Kevin S. Campbell

High-Speed Induction Motor with an Integrated Gearbox for Propulsion

Thesis submitted in partial fulfillment of the requirements for the degree of Masters in Science (Technology).

Espoo, May 29, 2017

Supervisor: Professor Kari Tammi

Thesis Advisor: Jenni Pippuri, D.Sc. (Tech.)

Author Kevin S. Campbell

Title of thesis High-Speed Induction Motor with an Integrated Gearbox for Propulsion

Degree program Master's Program in Mechanical Engineering

Major/minor Mechanical Engineering **Code** IA3027

Thesis supervisor Professor Kari Tammi

Thesis advisor Jenni Pippuri, D.Sc. (Tech.)

Date 29.05.2017 **Number of pages** 61 + 15 **Language** English

Abstract

Induction motors with a planetary gear are a viable option for the transportation industry as they are a relatively inexpensive electric drive solution. Designing a prototype of a high-speed induction motor with a planetary gear is the focus of this project. This will be the proof of concept, to demonstrate a compact and cost-efficient electric drive solution, when compared to electric drives with lower speeds and no gearbox. Using a high-speed electric motor and gearing it down will provide a high torque density and power. A prototype with a high power density and efficiency will provide a competitive alternative to other electric drive solutions.

The design choices of the prototype are covered. 3D modeling software is used for the mechanical design that integrates the planetary gear and the induction motor. Finite Element Method (FEM) simulations are completed to determine the final design. The geometry and properties of the induction motor are optimized using FEM. Electromagnetics, torque, and the losses of the induction motor are analyzed.

The prototype design presented in this thesis is analyzed to determine the overall efficiency, cost, and feasibility for the transportation industry. The design allows for future development by ensuring easy changes and additions that can be made to the prototype. The development of the high-speed motor should continue with the use of models and design presented in this thesis. The design presented in this thesis is another step towards the final prototype production. The possibilities for future thesis topics and improvements will be discussed at the end of this thesis. One possibility for future development is the use of additive manufacturing to build the induction motor.

Keywords Induction motor, manufacturing, design, electric vehicle, 3D modelling, planetary gear, FEM, Elmer.

Acknowledgement

I would like to thank everyone involved for allowing me the fantastic opportunity to learn more about high-speed induction motors. To Aalto University, for giving me the opportunity to further my studies in Finland.

I want to extend my deepest gratitude towards my thesis supervisor Professor Kari Tammi and thesis advisor D.Sc. Jenni Pippuri. Thank you very much for the assistance and time you dedicated to me during this work. The trust and courage you provided me was invaluable. The assistance from D.Sc. Jenni Pippuri, Jesse Mäntylä and D.Sc. Pavel Ponomarev was crucial to the work done with Elmer. I would also like to thank the transmission donor. Furthermore, the Henry Ford Foundation for financial support.

Finally, I would like to thank my family for all of the encouragement during my endeavors and time away from home. I could not have done it without your unconditional love and support. To all the friends I made during my studies, my time spend in Finland will be unforgettable thanks to all of you.

Espoo, 29.5.2017

Kevin Campbell

Table of Contents

Abbreviations and Symbols

B	Magnetic flux density [T]
I_s	Stator phase current [A]
J_s	Current density in the stator windings [A/m^2]
J_{slot}	Current density in the slot [A/m^2]
K_{Cus}	Space factor
N	Number of turns
N_{slots}	Number of stator slots
P	Power [W]
P_{in}	Power input [W]
P_{out}	Power output [W]
P_s	Shaft Power [W]
S_{cs}	Area of conductors in stator [m^2]
S_r	Area of rotor surface [m^2]
S_{us}	Area of the stator slots [m^2]
T	Torque [Nm]
U_{in}	Input voltage [V]
U_{ph}	Stator phase voltage [V]
Z_{Qs}	Number of conductors per slot
f	Frequency [Hz]
l	Length of machine [m]
l'	Equivalent length of machine [m]
m	Number of phases
n_m	Rotation speed of rotor [rad/s] [rpm]
n_s	Synchronous speed [rad/s] [rpm]
p	Number of pole pairs
r_r	Rotor radius [m]
s	Slip
δ	Air gap length [m]
$cos\ \theta$	Power factor
η	Efficiency
σ_{Ftan}	Tangential stress in the air gap [Pa]

2D	Two-dimensional
3D	Three-dimensional
AC	Alternating Current
CAD	Computer Aided Design
EV	Electric Vehicle
FEM	Finite Element Method
GUI	Graphical User Interface
HSD	Hybrid Synergy Drive
ICE	Internal Combustion Engine
PSD	Power Split Device
RPM	Revolutions per Minute
RTV	Room Temperature Vulcanization
SIF	Solver Input File

1 Introduction

1.1 Background

Electric vehicles (EV) are an immense field of research in today's society. Electrical motors are an integral part of this field. Induction motors convert 70-80% of all electrical energy into mechanical energy [1]. Induction motors with an integrated planetary gear can be utilized in the transportation industry for many reasons. These reasons include the fact that they can be a less expensive solution when compared to internal combustion engines (ICE) or even other electric drives. Additionally, induction motors have a simpler construction, which provides a higher reliability.

Induction motors are the most widely used electric motors in the world. They are easily available and can be considered the industrial workhorse. Induction motors tend to have a lower torque density when compared to permanent magnet motors and some other electric drive solutions [1]. This lower torque density leads to the potential of an induction motor with an integrated gearbox that can provide a sufficient torque density for the entire system. This could offer a viable option for the transportation industry, as an inexpensive and efficient solution. To obtain a high power density for the electric drive, a high speed of around 18,000 revolutions per minute (rpm) will be used. Clean, affordable, and reliable energy for transportation is something the world will benefit from.

1.2 Research Problem

Utilizing high-speed induction motors for propulsion can have some challenging aspects. Designing an induction motor that is optimized for size, cooling, power and torque is critical for practical use in transportation. Induction motors are used widely in applications like compressors. These applications have different design aspects when compared to transportation uses, such as considerably different operation profiles. The size of a typical induction motor can also make it less practical for transportation. These items need to be considered to make it a viable option for transportation.

Efficiency of high-speed induction motors is one of the greatest concerns and challenges to overcome. The efficiency of lower speed electric motors is generally higher, so making a more efficient high-speed motor is a priority to be a good comparison to other options. This would allow for smaller batteries, which delivers mass and cost savings. In addition, maintaining a price that will compare to, or be better than other options is of optimum importance to be competitive in the market today.

1.3 Objective

The objective of this project is to design a prototype of a high-speed induction motor with a planetary gear. The goal is to develop a compact and cost-efficient electric drive solution for the transportation industry. This prototype will be utilized to transfer electrical energy into physical motion of a vehicle such as a bus or automobile. This project is a proof of concept, that increasing the speed of a typical motor with a planetary gear will provide a higher torque density. Using the designed high-speed electric motor and gearing it down will provide those qualities. This will lead to savings related to the mass and space, both important aspects in vehicle design. Researching high-speed induction motors, planetary gears, and integrating the two will be completed to produce the finest prototype for research and investigation. The steps of designing a high-speed induction motor with an integrated planetary gear are

intricate and will be laid out in detail. Utilizing the resources available at Aalto University and the knowledge of colleagues will aid in the final prototype design.

1.4 Scope

The research is focused on the final prototype design of a high-speed induction motor. Items such as cost, final design, finite element method (FEM) simulations, cooling, and future development will be covered. The mechanical design will be completed with computer aided design (CAD) software, and the induction motor will be designed with the help of FEM simulations. Previously, partial electromagnetic design has been completed. Some smaller decisions will be made, such as using a solid or squirrel cage motor, winding layout, winding insulation, winding style and the exact air gap. In addition, the method for cooling the induction motor has to be developed.

The thesis will be broken down into six sections. The introduction, state of the art, methods, results, discussion and conclusion. State of the art will review all of the relevant information regarding induction motors and planetary gears. The methods section will discuss the steps taken to finalize the design. In addition, everything required and used for the process will be discussed. The results will cover the outcome of this project, including the simulation results, final 3D model design and electric motor design. The discussion will review the items that can and should be done in the future, as well as what could have been done differently for this project. The conclusion will give a brief synopsis of everything determined in the paper.

2 State of the Art

This section is designated to explain the working principles behind the main components used for this thesis. This will include what research has been done with other projects relating to induction motors and planetary gears.

2.1 High-Speed Induction Motors

This section will give a summary of high-speed induction motors. When a motor has speeds of over 150 m/s, the motor is considered a high-speed motor [2]. Induction motors or asynchronous motors are used in a wide variety of applications today. The working principle behind an induction motor is widely known. There are two main parts to an induction motor, a stator and a rotor. The rotor will produce the final torque or output of the machine. The stator has electrical windings that will have an alternating current (AC) supplied to it. This creates a rotating magnetic field that will rotate with the frequency of the AC supply. According to Faraday's law of electromagnetic induction, this field will induce a current into the short-circuited rotor winding. This will create another electromagnetic field. This will cause the rotor to rotate in the direction of the stator's magnetic field. Synchronous speed is the speed that the stator electromagnetic field rotates. Synchronous speed is defined as

$$n_s = \frac{60f}{p} \tag{1}$$

where f is the supply frequency and p is the number of pole pairs. Induction motors work at a speed that is a little less than the synchronous speed. The difference between the synchronous speed and the rotor rotation speed is called the slip. Slip is defined as

$$s = \frac{n_s - n_m}{n_s} \tag{2}$$

where n_s is the synchronous speed and n_m is the rotation speed of the rotor. This will typically be given as a percentage, so the final number should be multiplied by 100.

Permanent magnet motors and induction motors are some of the most common types of motors used for electrical applications today [3]. These are used for a wide variety of reasons. Permanent magnet motors are more common in the automotive industry. Permanent magnet motors are more expensive and are not as mechanically rigid as induction motors. For these reasons, the induction motor is used in this thesis.

The efficiency of electric motors is an important aspect to study. The more efficient the motor is, the more reasonable and cost effective it could be for transportation. Reducing the amount of electromagnetic and mechanical losses in an electric motor is one way to improve the efficiency. Efficiency η is

$$\eta = \frac{P_{out}}{P_{in}} \tag{3}$$

where P_{out} is the output power and P_{in} is the input power. High-speed motors have a larger power density and loss-density, so implementation of a proper cooling system is key to reduce the amount of losses from heat [4].

The losses in a high-speed machine are an important consideration in the design process. Figure 1 lists most of the common types of losses to consider during the design of an induction motor. According to [5], the power density of a high-speed machine could be three times higher than a standard machine. With that factor, and less cooling area, the machine needs to have adequate cooling designed into the system.

The first type of losses are electromagnetic. Winding losses are due to the resistance in the conductors that are dispersed through the stator and rotor slots. Next, are core losses; these are the losses that occur in core material of the machine. These can also be called iron losses, as most of the cores are made of iron or a ferromagnetic material. The core losses are due to a changing magnetic field. Furthermore, the core losses can be broken down into hysteresis losses, eddy current losses, and excess losses.

In addition, some other types of electromagnetic losses are harmonic losses and eddy current losses. Eddy currents are produced when electrically conducting machine parts are subjected to changing magnetic fields. Harmonic losses come from the design of the rotating machine. These come from stator and rotor slot harmonics, and the converter utilized to power the machine. It is critical that the converter provides as sinusoidal voltage supply as possible to reduce losses [6].

Next, are of the losses due to the mechanics of the machine. The most common types of mechanical losses are due to friction, from items such as the bearings and gearing. The bearings and gearbox needs to be adequately cooled and lubricated to reduce friction losses.

These losses are dissipated as heat. This is why the cooling of high-speed machines is essential. The higher operating frequency and speeds cause higher operating temperatures, therefore the possibly of losses from heat are higher. More information about losses can be found in the previous thesis [7].

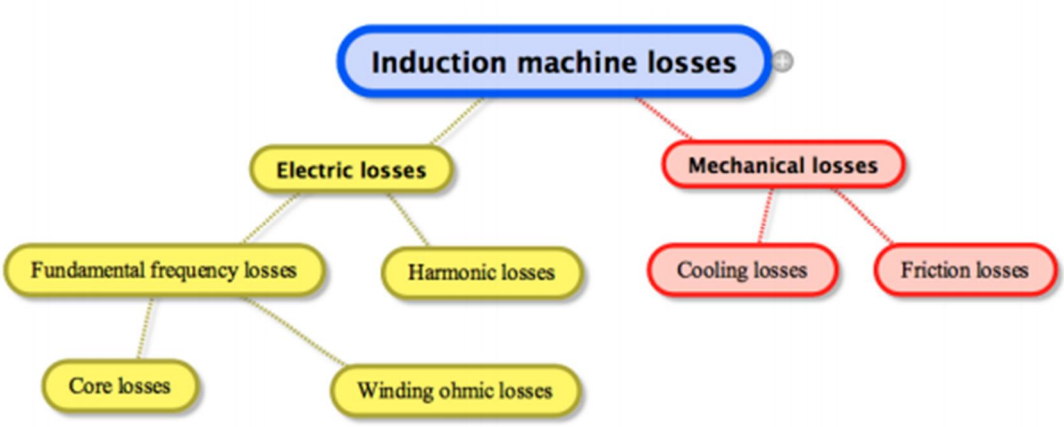

Figure 1: Flowchart of losses in an induction motor [5]

The stator is the stationary part of an electric motor. Stators are usually made from thin slices of electrical steel or iron 0.1 to 1 mm thick. Electrical steel provides a higher electric resistivity. From [8], choosing the thinnest sheets possible will reduce eddy current losses. The steel used is magnetic, and has good properties for electromagnetic induction. Hundreds of these thin steel sheets or laminations will be placed together to make the final structure of the stator, as seen in Figure 2. Each lamination has multiple slots for the electrical winding to pass through. The shape and size of the slots should be optimized for each specific application. This can be done, for example, using simulations with FEM software. Additionally, determining the number of slots used in the stator is another crucial parameter. The overall size or diameter of the stator can help determine these characteristics. The stator yoke is the material above the stator slots. The yoke affects the flux density of the machine. Although using electrical steel laminations are beneficial from a magnetization point of view, they are expensive to make and are not as structurally sound as a solid piece of material. Luckily, the stator does not rotate. Thus, there are typically low stresses and forces during operation.

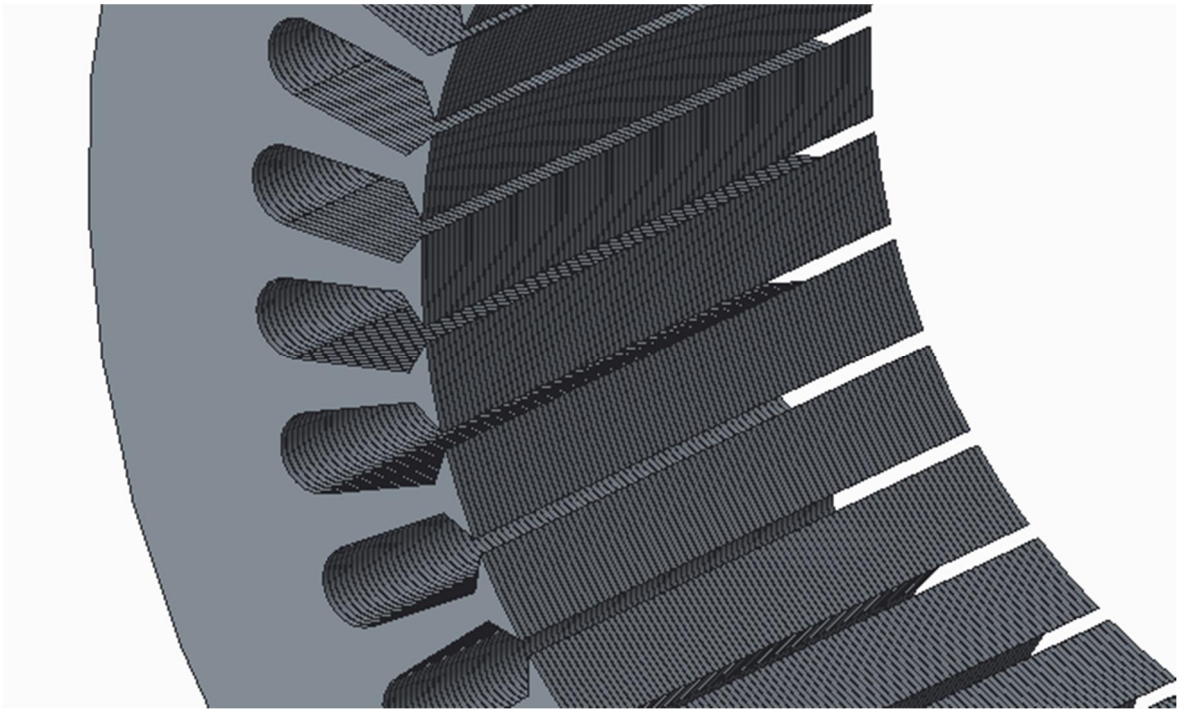

Figure 2: Stator lamination stack

The windings in an induction motor are key to the operation and efficiency of the system. There are many different winding layouts possible. Distributed windings reduce the harmonics and provide better efficiency values. Concentrated windings are another common type of winding. They also have higher noise and vibrations than distributed windings [9]. Distributed windings use one conductor wire passing though many different stator slots and multiple poles of the machine. Concentrated winding layouts use one conductor wire wound around one tooth of the stator and only one pole of the machine. These layouts are shown in Figure 3.

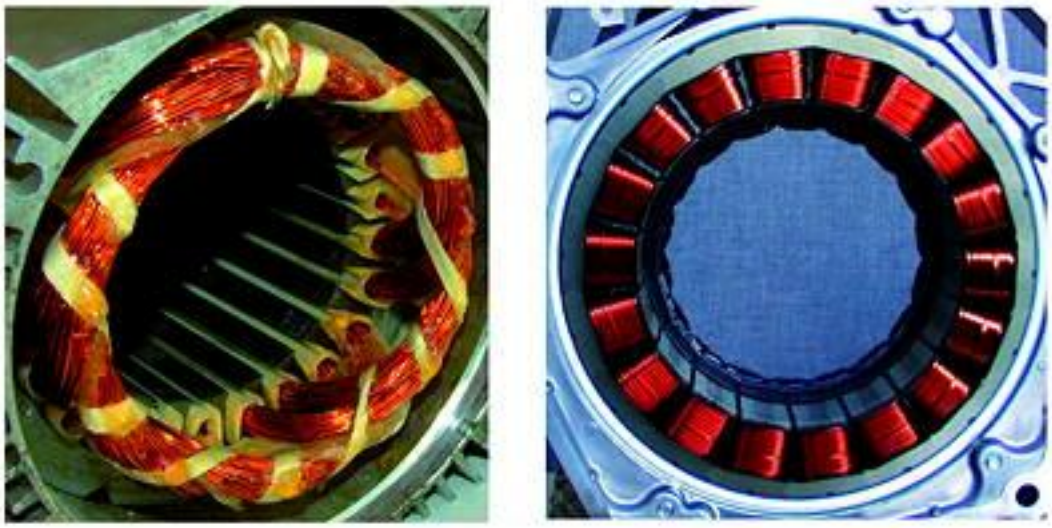

Figure 3: Distributed vs. concentrated windings [10]

Double layer windings are common practice for induction motors. Double layer windings place one coil side on the top of one slot and on the bottom of another slot. Essentially, this divides each slot into half to make double layer windings. Single layer windings use one coil side for the whole stator slot. Multiple coil sides can be placed in each slot for double layer windings [11]. This can be better visualized in Figure 4 and Figure 5. Double layer windings are often used to reduce the high-frequency losses. According to [12], a well-designed multi-layer design can have fewer losses than single-layer windings, although it is crucial for it to be intricately designed and not randomly put together.

Fractional windings use a fractional number of slots per pole and phase; this will not be used in the design presented. If the windings are not fractional, then they are considered integer windings. Furthermore, short pitching can be used. Short pitching is when one slot has conductors from two different phases; this also provides smaller end windings. The end windings are the visible conductors seen at the end of the machine. The end windings are used to loop the conductors to the next desired slot.

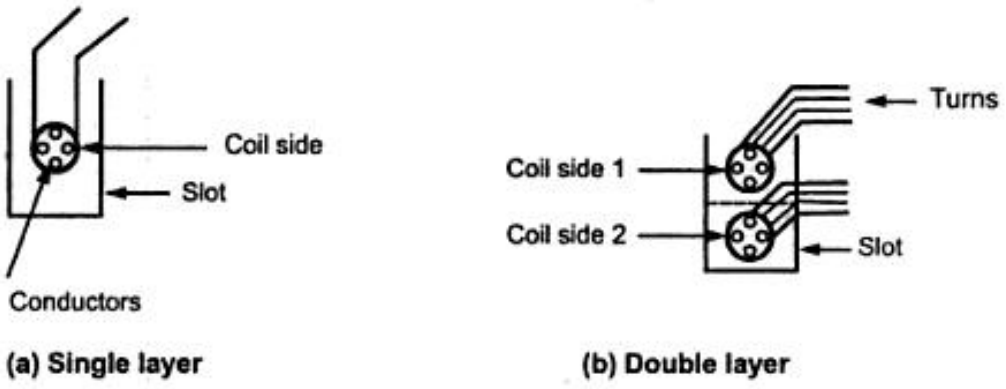

Figure 4: Single layer vs. double layer windings [13]

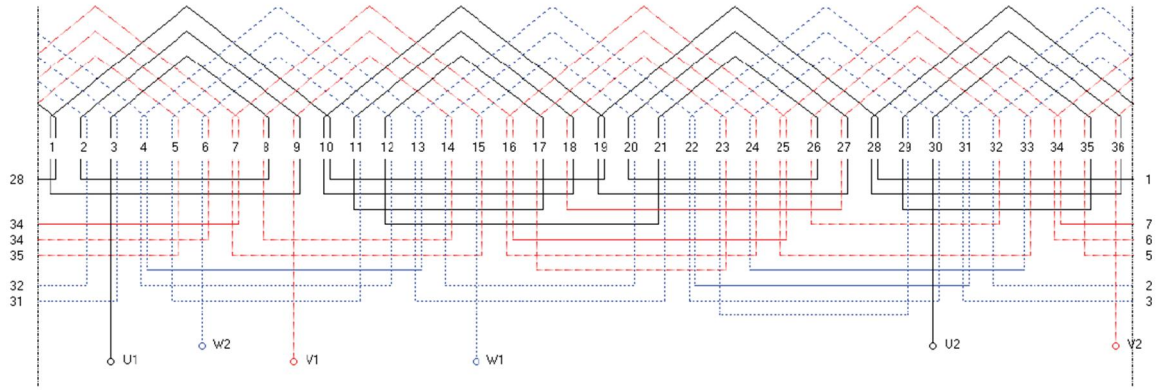

Figure 5: Double layer winding layout for 36 stator slots [11]

Using the right conductive material for the windings is important to minimize the losses, as the material has to handle the operating temperatures. Filling the stator slots compactly with a highly conductive material such as copper allows for higher power densities. The windings inside the stator slots will be placed inside of an insulation material. This will provide thermal insulation from the stator material and the thermals created from the other windings. It is best to fill the slots with epoxy to fill the empty space and so the conductors stay together. In addition, after the windings have been installed, a wedge can be placed at the stator slot opening to keep them in place.

Induction motors can be connected in two different ways, star and delta configurations. Star connected motors have one end of each coil connected at a common point; this is called the neutral point. In delta connections, one end of each coil is connected with the start of another coil. In star connected motors, the line current is equal to the phase current. The line voltage is √3 times the phase voltage. In delta connections, the line voltage is equal to the phase voltage. The line current is √3 times phase current. Star connections generally do not require as much insulation as delta connections. In addition, star connected motors can take a lower current to produce a higher torque [14]. However, most 3-phase induction motors are delta connected.

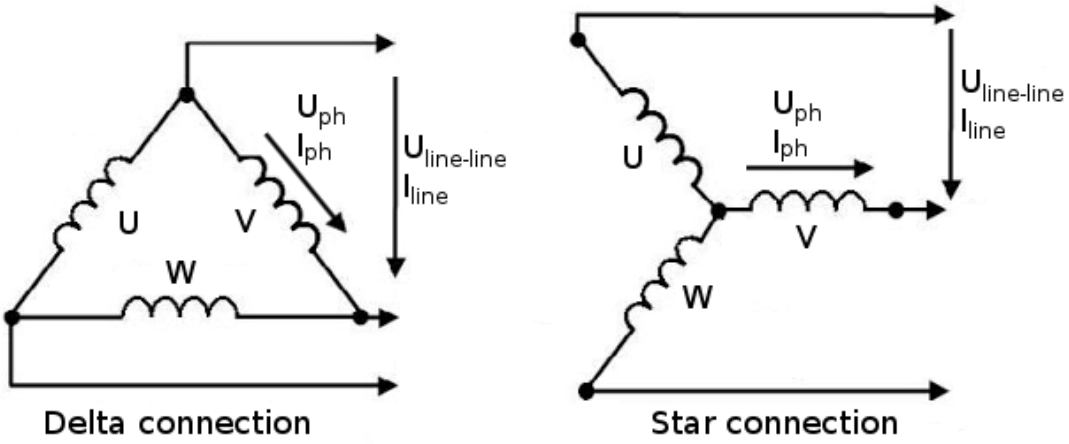

Figure 6: Delta and star connections [15]

The thermal properties of the stator and rotor are one of the most critical areas of concern when designing the induction machine for high-speeds. Designing a high-speed induction motor is a demanding task. Many values have to be determined, and these can have a major

influence on the properties and performance of the motor. Typically, induction motors are air cooled by a fan that is connected to the shaft of the spinning rotor. This will allow airflow through the system that travels through the air gap. This allows convection to reduce and maintain an ideal operating temperature. Conduction also occurs from the rotor to the bearings. In addition, determining the ideal material for the rotor can reduce the thermals. Copper, aluminum and steel provide high thermal conductivity [16].

The rotor is the rotating part of the electric machine. Multiple constructions can be used for the rotor. For high-speed applications, solid rotors will provide the best option due to their mechanical durability, reliability, manufacturing costs, and low level of vibrations [8]. Using a laminated rotor would provide more electromagnetic benefits and can have a 2 - 3% higher efficiency when compared to solid rotors [17] [18]. However, any unexpected stresses or balancing issues would present themselves faster in a laminated type rotor. Solid rotors are made with one large piece of ferromagnetic material. The simplest solid rotor construction is a smooth cylinder, but this has electromagnetic properties which are not always ideal [8]. Improvements have been made on the smooth rotor in an attempt to improve performance and electromagnetic characteristics. The other types of solid rotors are slitted, slitted with end rings, squirrel cage, and coated smooth. These rotor constructions can be seen in Figure 7. Each one of these constructions is more difficult to manufacture and therefore, more expensive than a solid smooth rotor. Solid slitted rotors help guide the flux into the rotor and reduce eddy current losses. Unfortunately, slitting can also increase the air gap friction losses [19]. This type of rotor is becoming increasingly more common for high-speed machines.

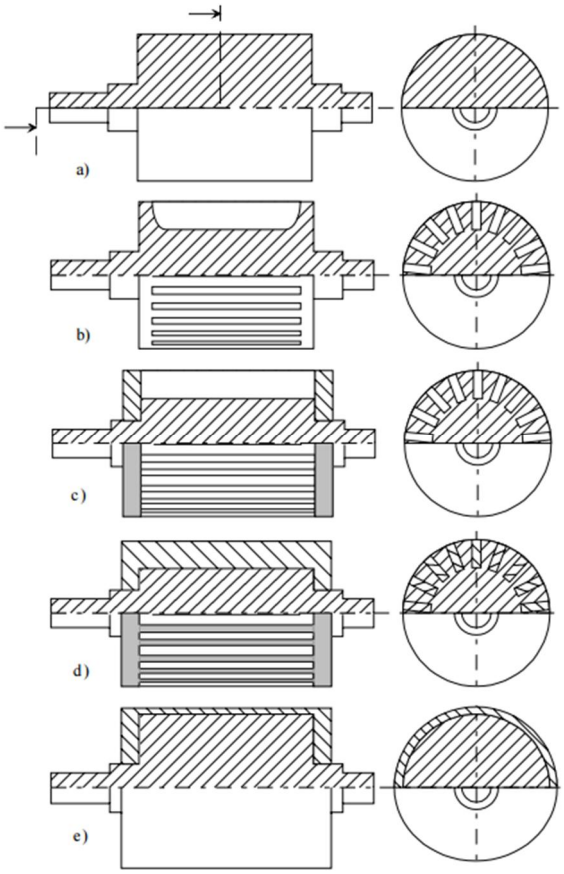

Figure 7: Solid rotor constructions: a) smooth, b) slitted, c) slitted with end rings, d) squirrel cage, e) coated smooth [8]

The air gap is another crucial element to the overall efficiency of an induction motor. The air gap is a small space between the rotor and stator. This will typically be no larger than 4.0 mm. This gap serves multiple purposes. First, it allows convention of air from the rotor. Second, it allows air to flow through the machine. This will provide cooling for the electrical machine. This small space is also, what allows the rotor to spin without any interference. The air gap also plays a huge role in the magnetization. The size of the air gap determines a number of items in the motor. In order to decrease harmonics and overall losses in the rotor is it necessary to have a sinusoidal air gap flux. Selecting the best air gap size is essential to determining a way to minimize the overall losses in the motor. Choosing a larger air gap is the standard for high-speed induction motors [17].

All of these components from an electrical machine that were explained above can be seen in Figure 8.

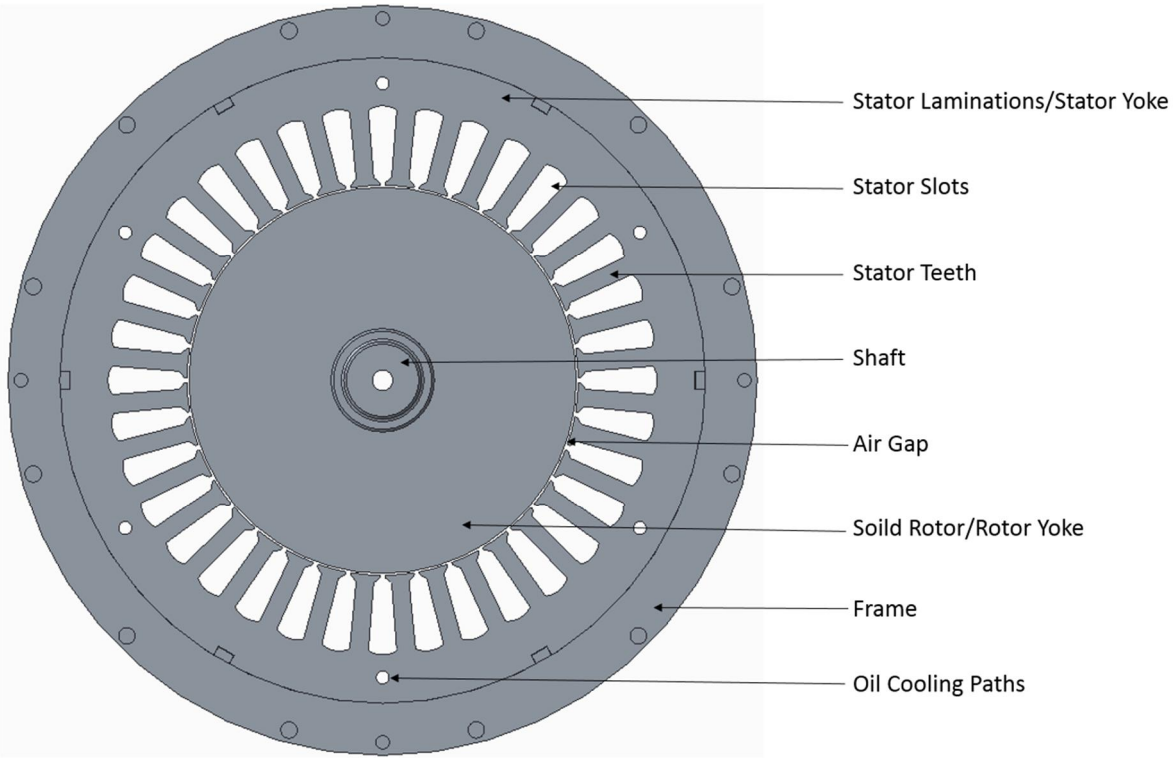

Figure 8: Components of a typical induction motor

Rotating at high-speeds is a process that must be handled delicately. Using the proper bearings for this application is vital to maintain proper rotating speeds without causing problems in the future. The bearings also have a significant influence on the efficiency of the motor due to mechanical losses that come from the high rotation speeds.

The frame of the induction motor is the part that houses all of the other components of the machine. Furthermore, it allows for stable mounting of the system. The wiring interface is also housed in the frame. It allows the complete package to be delivered fully assembled.

The asynchronous AC machine talked about in this thesis will require a frequency converter for operation. The primary reason a converter is required is to convert a fixed frequency and voltage to a variable frequency and voltage. Essentially this allows for speed control of the

motor. In addition, the converter will convert the incoming direct current power to alternating current power used by the induction motor.

2.2 Planetary Gears

The idea of planetary gear trains have been used for a long time, dating back to the second century. A planetary gear train consists of four major components. These are the sun gear, planet gears, planet carrier and the ring gear. Typically, one of the three gears is constrained not to rotate, which is normally the ring gear. In this case, the sun gear is the input gear and the planet gears are the output of the system through the planet carrier. The planet gears are connected with a planet carrier. This configuration of the gear train provides an output speed that is reduced from the input.

These gear trains can evenly distributed the load and stress applied. The multiple points of contact allow of the load to be shared in multiple locations. As a result, planetary gears are very strong and reliable. The teeth of the gears are typically designed in one of two ways, using helical gears or spur gears. Helical gears are the standard today because the two mating gears will have a larger contact surface area when compared to spur gears.

Planetary gears can be used in multiple configurations. Depending on which gear is held stationary will provide different results. Figure 9 shows what can occur for each specific case.

Sun Gear	Carrier	Ring Gear	Speed	Torque	Direction
1. Input	Output	Held	Maximum reduction	Increase	Same as input
2. Held	Output	Input	Minimum reduction	Increase	Same as input
3. Output	Input	Held	Maximum increase	Reduction	Same as input
4. Held	Input	Output	Minimum increase	Reduction	Same as input
5. Input	Held	Output	Reduction	Increase	Reverse of input
6. Output	Held	Input	Increase	Reduction	Reverse of input
7. When any two members are held together, speed and direction are the same as input. Direct 1:1 drive occurs.					
8. When no member is held or locked together, output cannot occur. The result is a neutral condition.					

Figure 9: Planetary gear operation [20]

The most common material for planetary gears is steel. Although, for applications with less loads, plastics have become widely used for servomotors.

Planetary gears can be compounded to provide alternative solutions. This is most commonly seen in transmissions. This can allow for even more variation in gear ratios. Planetary gears are most commonly used in automatic transmissions. Typical input speeds of planetary gears for transmissions are around 10,000 rpm. Since planetary gears can rotate at such high speeds, vibrations can be present.

2.3 Electric Motors and Planetary Gears

Combining these two systems could potentially provide a promising alternative for electric drive systems. This area has not been studied largely; it could provide a cheaper system with ideally the same efficiency as a permanent magnet motor. Using a high-speed induction motor with a planetary gear can improve the overall torque density throughout all of the

different operating speeds. An initial prototype design was visualized in Figure 10 from [21]. This is the basis for the mechanical design presented in this thesis.

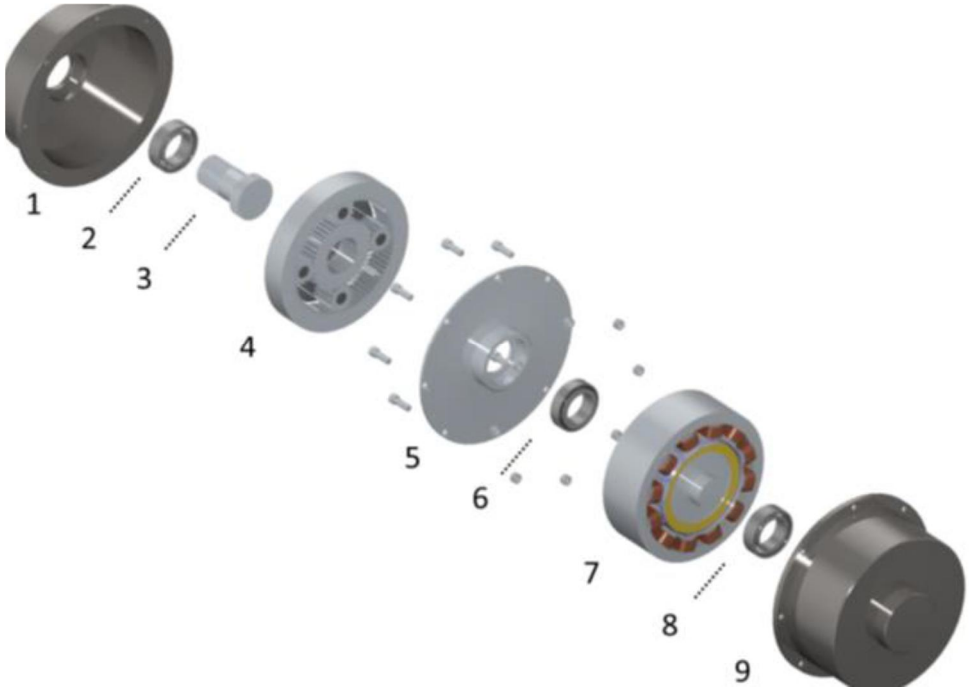

Figure 10: Initial prototype design [21]

Utilizing electric motors with planetary gears is not necessarily a new system. They are common in a few types of situations. First, small electric motors, such as stepper motors are used in conjunction with small planetary gears. Second, the *Toyota Prius* is widely known for using electric motors in conjunction with a planetary gear. The system used in the *Prius* is called a *Power-Split Device* (PSD) and *Hybrid Synergy Drive* (HSD). However, the motors used in the *Prius* are synchronous permanent magnet motors and are expensive. In addition, this system is combined with an internal combustion engine and is not a fully electric vehicle. This method is much more complicated and expensive when compared to using an induction motor with a planetary gear. The application investigated in this thesis will be fully electric.

The *Prius* is a hybrid vehicle, and as stated, uses an electric motor with an ICE. Hybrid electric vehicles are quite common in today's market. One of the main benefits of hybrid vehicles is their fuel efficiency. In addition, they also provide higher performance and lower emissions than standard internal combustion engines. Many different drivetrain configurations can be used in hybrid vehicles to provide different qualities. This includes using different types of electrical motors such as induction motors, permanent magnet motors and switched reluctance motors. The three main types are series hybrid, parallel hybrid and series-parallel hybrid drivetrains. In series hybrid, the internal combustion engine and electric motor are ran in line so the electric motor is the only thing providing power to the wheels. The parallel hybrid system is when the electric motor and internal combustion engine are directly coupled through something like a gearbox. They are both supplying torque to the wheels. Series-parallel hybrid drivetrains are used in conjunction with a planetary gear to allow the wheel speed to be removed from the engine speed [22]. This is the type of system used in the *Toyota Prius*. This allows either one of the power sources to be used separately or together. The PSD and HSD used in the *Prius* allows for five different

driving modes. These include, starting out, normal driving, full acceleration, deceleration and reverse [23].

General Motors has been working with electric vehicles for a long time. From as early as 1964, they have been testing three-phase induction motors for electric vehicles. These electric vehicles run at speeds up to 13,000 rpm and 137 horsepower [24].

Another example of electric motors used with gearing is the *Chevrolet Bolt* EV. This system uses an electric permanent magnet motor in conjunction with a transmission. The electric motor provides 97% efficiency. It utilizes a trademark bar-wound stator and a double-layer of magnets in the rotor. The 150 kW motor, that has a maximum speed of 8810 rpm is the only power source for the vehicle. The gear ratio in the *Bolt* is 7.05 [25]. This system is similar to the system designed for this thesis. However, it does not use a planetary gear and uses a higher gear reduction.

Many modern electric vehicles are simply direct drive and do not require any additional gearing. For example, this system is used in all current electric vehicles designed by *Tesla*. The *Tesla* uses a high-speed induction motor [26].

Stepper motors are often used in conjunction with planetary gears. They utilize high speeds and low gear ratios in the gear train, which provides maximum torque. Torque is one of the most sought after qualities in a stepper motor. This system provides similar qualities desired for the project at hand. However, stepper motors are small, commonly use permanent magnet motors, and are not designed to rotate continuously. They are designed to rotate to a precise position and stop for accurate placement of the attached component.

This project will combine the ideas from some of the aforementioned systems and some new ideas for a system that will provide high torque density at operating speeds designed for automobiles.

3 Methods

Taking a scientific concept to a reality can be a challenging process. This section will layout the procedures that went into designing the prototype, from simulations to 3D modeling.

3.1 Design

The principal design choices will be explained in detail. The process to design a rotating electrical asynchronous machine is an exacting task. The proper design process is important to achieve the best efficiency possible. Figure 11 shows the typical design process and the relevant values that need to be determined.

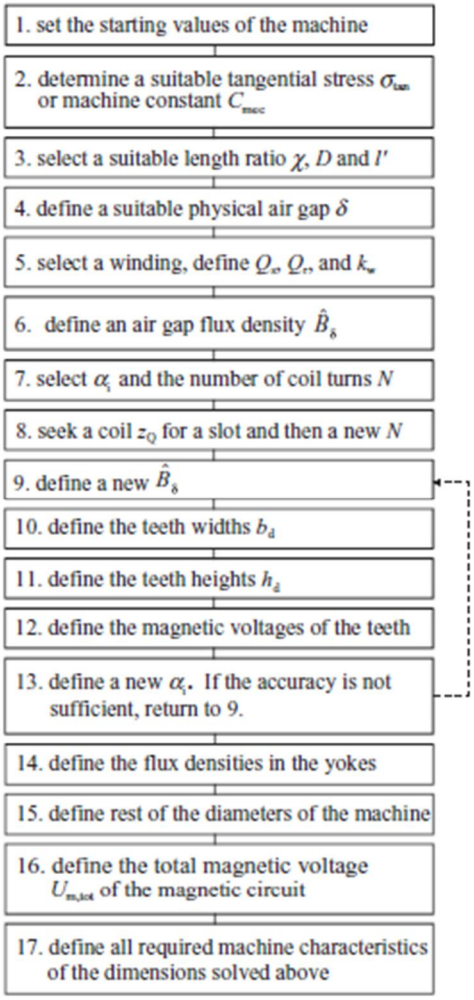

Figure 11: Design process for an asynchronous machine [4]

3.1.1 Previously Developed Work

Two theses have been completed related to this project. Partial electromagnetic simulations were done to determine some influencing factors in the design. This work is the basis for this thesis, and is used to determine many factors for the design. This work can be found at [7]. Additionally, the rotor dynamics were analyzed [27]. This work shows the vibrations, natural frequencies, critical speed, bending modes and centrifugal forces of the rotor design.

The goal of this thesis is to collect the previously completed work, and the work completed in this thesis to finalize a design that will be used for prototyping and proof of concept.

3.1.2 Dimensions and Requirements

Designing this system for transportation purposes means that the system has to be capable of highway speeds. A goal of around 100 km/h was set for this electric vehicle. In an application of a city bus, the max speed would be 80 km/h. A tire diameter of 0.9 to 0.95 m and a circumference of 2.8 to 3.0 m was used. 100 km/h is roughly 27 m/s. With these values, the rotations per minute were calculated to be around 600 rpm. The final gear ratio from the transmission to the final speed of the wheels in similar applications is between six and seven. This provides a speed of around 4,000 rpm. With a planetary gears reduction ratio between two and four, this leads to a speed of around 16,000 rpm, and when accounting for some margin in the speed, a value of 18,000 rpm was determined. State-of-the-art motors are increasing the overall top speed, the *Prius* has moved from a speed of 10,000 rpm to 14,000 rpm [23]. Electric motors in newer EV's are trending to increased speeds above 18,000 rpm, such as the EV's made by *Tesla* [26].

Below is an initial design specification list for the integrated electrical motor and gear of this project. These items have been previously determined [7]. Adjustments to these values will be made for the final design.

- Machine type: Induction machine
- Type: Radial flux
- Rated power: 150 kW
- Maximum rotational speed: 18,000 rpm
- Maximum rotational speed after gear: 6,000 rpm
- Slip: 2%
- The number of poles: 4 (2 pole pairs)
- Rated frequency: 600 Hz
- Number of phases: Three
- Outer diameter of the stator: 250 mm
- Length of the stator: 80 mm
- Outer diameter of the rotor: 150 mm
- Air gap length: 0.7 mm
- Stator slot height: 25 mm
- Stator slot width: 10 mm
- Stator slot opening: 2 mm
- Number of stator slots: 36
- Stator yoke thickness: 36.8 mm
- Rotor type: Solid
- Winding layout: Double-layer and distributed

3.1.3 Air Gap

For a 50 Hz asynchronous machine, the air gap length δ can be estimated by:

$$\delta = \frac{0.18 + 0.006 \times P^{0.4}}{1000} \tag{4}$$

where P is power in watts. This equation is designated for machines with the number of poles pairs greater than one. As this equation is designed for 50 Hz machines, it will not give a perfect air gap length for this project. In addition, this equation is only designed to give a starting point for the air gap; changes should be made after determining what qualities are desired for the machine being designed.

Using a power of 150,000 watts, the air gap can be calculated to be 0.885 mm. When comparing this to the air gap determined from previous simulations it shows that the size is similar. This machine is designed for a frequency much higher than 50 Hz, so there should be a difference between the values. However, there is no absolute way to calculate the air gap length. Simulations are the best way to determine the air gap. The starting point for the air gap is 0.7 mm based on the work completed in [7].

In high-speed machines, the air gap is typically larger than lower speed machines to mitigate losses. The air gap should be designed for high-speed and high frequency operation. An air gap of 3.0 mm is quite common for machines with similar designs as the one presented in this thesis. After conferring with some colleagues in expert interviews, it was determined that the air gap should be increased by a large margin. The calculated value of 0.885 mm and simulated value of 0.7 mm are too small. The new air gap value will be 3.5 mm for the final design. When comparing this to similar machines with higher frequencies, the air gap was similar, as seen in [5] and [17]. The previous air gap would be in the right range for a machine with normal frequencies and speed, for example in [17].

Increasing the air gap also has beneficial impacts on the machine. The rotor iron losses are decreased, the mechanical stability is increased, and additional losses are reduced [28]. However, the stator winding losses and power factor are decreased.

3.1.4 Rotor

A cylindrical solid rotor was chosen for this design as it is the most suitable for high-speed applications [4]. This is because it was determined that having a more mechanically robust structure will be better for the development. Using a short rotor with a large diameter is better for high-speed applications to reduce vibrations [5].

There are multiple choices to be made when designing the rotor. What material to use, should the rotor be slitted, should the rotor be coated, should the rotor be solid or laminated, and how to keep the rotor cool. Induction machines running at the operating speed will create a lot of heat. It is common practice for high-speed machines with solid rotors to have slits or machined groves in the surface of the rotor to help with cooling and magnetic inductance. When using axially slitted rotors, the width can start at around 2.0 mm and the depth of the slit should be half of the rotors radius [29] [30]. Increasing the depth of the slits any more will result in a decrease of torque.

A solid rotor construction has been chosen for the purposes of this thesis. This will allow for easy development and manufacturing in the early stages. The rotor will be milled from a solid piece of ferromagnetic steel. Slits will also be added to the rotor for cooling and improved magnetization. The design will made with 30 slits in the rotor. This design is shown in Figure 12. It is recommended to have between 5 and 15 slits per pole pair [5]. Without the slitting, the magnetization characteristics of the rotor are poor. During the process of getting electrical steel sheets cut for the stator, there will be cylindrical pieces cut

from the inside on the stator that can be made into a laminated rotor if desired. These pieces will be kept in the event that a laminated rotor is designed.

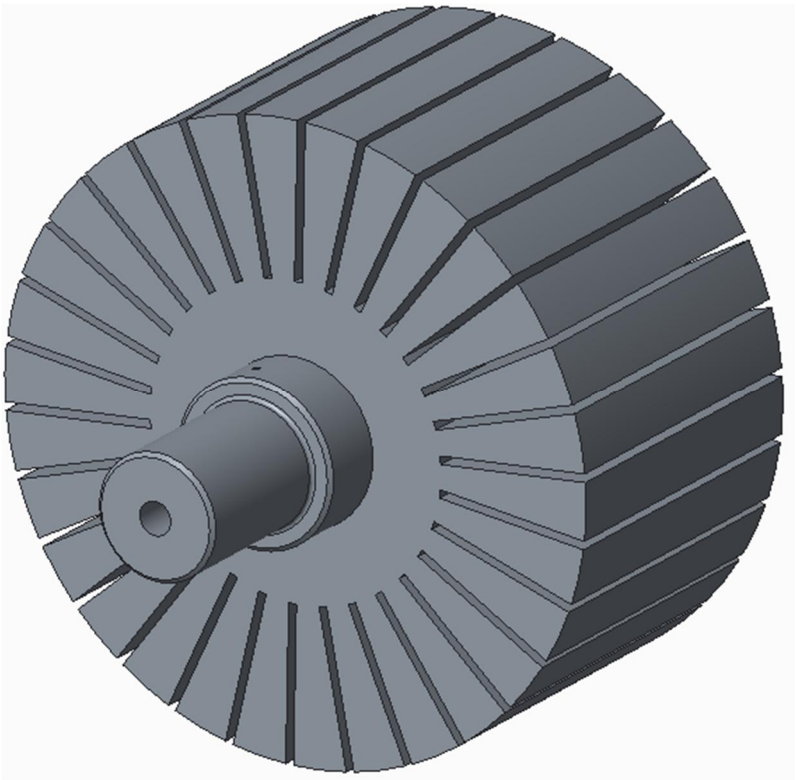

Figure 12: Rotor design with 30 slits

The outer diameter of the rotor is 150 mm. The rotor shaft will input power to the planetary gear. The size of the shaft is made to fit the chosen bearings for the system, which are discussed in section 3.1.6. The shaft used in this design is made from the same material as the rotor for simplicity purposes. The entire rotor and shaft is designed to be milled from a solid piece of metal. When done on a lathe, deviations to the rotor and shaft shape can be reduced; this will provide a cylindrical shape and reduce vibrations. The design was chosen this way, because if made into two pieces, the two would need to be mated by welding, end rings or something similar. This would not be ideal for the initial design; extra vibrations could be present, and is not as structurally sound as a solid design. However, making a two-piece rotor is possible, and would present the possibly for using a different material for the shaft. The shaft length is 167 mm. The shaft is shown below in Figure 13. Once inserted into the planetary gear, this leaves a 5.0 mm spacing between the end of the shaft and the inside of the planetary gear. This also provides room for small changes in placement. The shaft has a center hole drilled the entire length for oil to travel through and enter the planetary gear. This is the main source of cooling for the planetary gear. Each end of the shaft has been made to the same diameter of the bearings used to support the rotor. Small air vents have been drilled into the shaft for airflow.

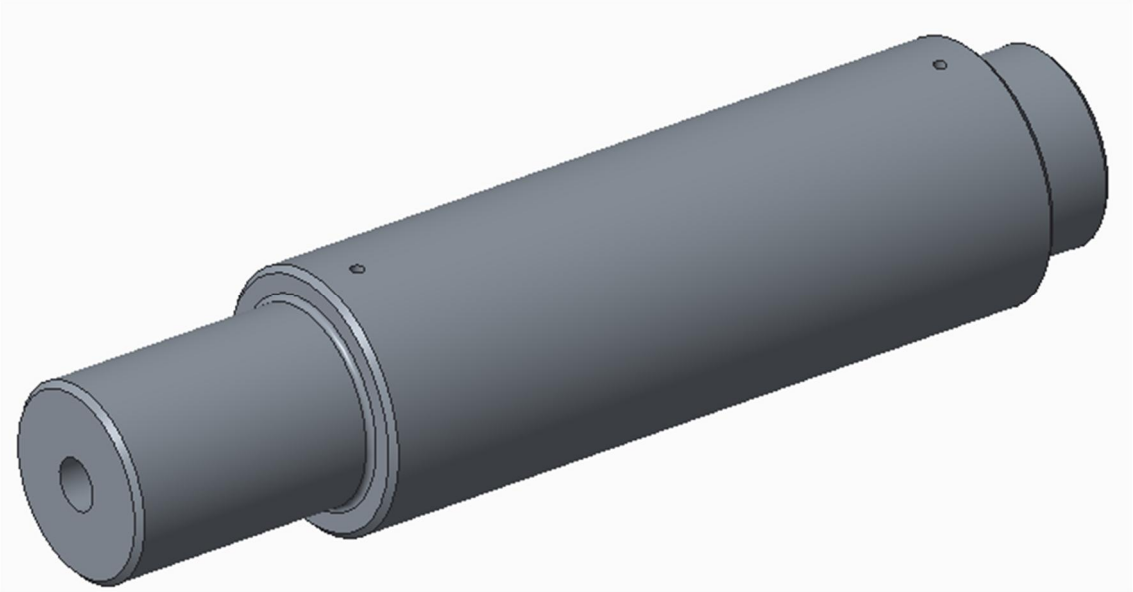

Figure 13: Rotor shaft

The material used for this rotor will be ferromagnetic steel Fe52. This material has proven to be the standard for solid rotors. This material was also utilized in a high-speed solid rotor induction machine from [5].

The torque produced from the machine is a key characteristic. The torque provides information on how powerful the motor is, and if it is strong enough to drive an electric vehicle. First, the tangential stress σ_{Ftan} is determined from common values of induction motors. For our purposes σ_{Ftan} = 21500 Pa [4]. Next, the required torque T was calculated. The torque T is

$$T = \sigma_{Ftan} r_r S_r \tag{5}$$

where r_r is rotor radius and S_r the area of rotor surface. The area of rotor surface is

$$S_r = 2\pi r_r l' \tag{6}$$

where l' is the equivalent length of the machine. Equivalent length l' is

$$l' = l + 2\delta \tag{7}$$

where l is the length of the stator and δ is the air-gap length.

Using the equations listed above, the required Torque is 66.10 Nm. This result is similar when compared to simulated results found previously [7].

From [27], many aspects of the rotor design have been checked and verified. First, the natural frequencies were obtained. The first bending mode was found to be around 6,000 Hz, and even higher for the second and third. It should be noted that the high values of the bending modes are expected to be higher with a rotor of these dimensions. Second, the critical speed was determined of the rotor with the addition of some bearing stiffness values. With minimum recommended stiffness value of 50 kN/mm, the critical speed was determined to

be 23,000 rpm. Additionally, using a higher stiffness value of 100 kN/mm, the critical speed was 31,000 rpm. Finally, the centrifugal force was analyzed. At the maximum rotational speed of 18,000 rpm, the force was about 75 kN. This lead to a higher Von-Misses Stress, with an absolute maximum value of 90 MPa. After this detailed analysis, it was believed that the rotors characteristics are satisfactory for the operation in this induction machine. Detailed information about these analyses can be found in [27].

3.1.5 Stator and Windings

Determining the correct dimensions of the stator is a critical component to obtaining ideal properties of an induction motor. Determining the dimensions started with the stator and rotor outer diameters. The stator outer diameter was known to be 250 mm so the machine would not be too large for use in the automotive industry. The rotor outer diameter was known to be 150 mm. The best diameter ratio from the outer to inner diameter of the stator is 0.6 [4]. The stator outer diameter is 250 mm and with the addition of the air gap to the rotor diameter, the stator inner diameter is 157 mm. This provides a ratio of 0.628.

Finite element simulations are used to determine the dimensions of the stator slots, stator teeth and stator yoke. Different geometries can be simulated to identify the ideal shape of the stator. By analyzing the magnetic flux densities and torque, the best shape can be found. The second stage is to perform simulations with the current density supply and voltage supply. Additionally, the motion of the motor will be included to provide the most accurate to real life test results.

A crucial design aspect is the size of the electrical steel sheets. The thickness of the material is determined based on availability, cost, and the magnetic and mechanical characteristics desired. High frequency applications can make choosing a suitable material difficult. Materials with high amounts of silicon can lead to brittleness, and materials with high amounts of aluminum have a high Vickers hardness value and a high resistivity that can be used for special applications [4]. Iron with small amounts of Cobalt can be used at a higher price point, but can provide better strength [31]. Choosing the material should first be done by checking availability, as it can be difficult to procure the desired material and thickness. The electrical sheet will be sent to a water jet to get the exact shape of the stator cut out.

During the design of the stator, some important information from expert interviews was determined. The wire thickness should be small, around 0.6 mm. The thickness of the electrical steel sheet should be between 0.2 and 0.35 mm. All of the losses from the stator and rotor should be calculated using FEM. In addition, the air gap should be large and there should be temperature sensors in the machine. All of these items have been implemented into the design process.

The method to calculate values of the current densities, space factors, number of turns and the number of conductors per slot can be seen below. It should be noted that values calculated using these equations are designed for a starting point. The values are subject to change with multiple iterations and simulations to achieve the desired results. The shaft power P_s is

$$P_s = 2\pi T \frac{n_m}{60} \tag{8}$$

where n_m is the rotation speed of the rotor at 17,640 rpm assuming a 2% slip. The stator phase current I_s is calculated by:

$$I_s = \frac{P_s}{m\eta U_{ph} cos\theta} \tag{9}$$

where m is the number of phases, the target efficiency η value is 0.95, U_{ph} is the stator phase voltage, and cos θ is the target power factor at 0.8. In star connection, the phase voltage can be calculated by:

$$U_{ph} = \frac{U_{in}}{\sqrt{3}} \tag{10}$$

where U_{in} is the voltage fed to the machine by the converter. For our purposes, it is 500 volts. Next is the area of the conductors in the stator S_{cs}:

$$S_{cs} = \frac{I_s}{J_s} \tag{11}$$

where J_s is the current density in the stator conductors. The current density value is typically between 3-8 A/mm^2 [4]. The area of the stator slots S_{us} is:

$$S_{us} = \frac{Z_{Qs} S_{cs}}{K_{Cus}} \tag{12}$$

where K_{Cus} is the space factor for the stator winding. The previous equation can be used to calculate the number of conductors per slot Z_{Qs}. Finally, the current density in the slot can be calculated J_{slot}:

$$J_{slot} = \frac{Z_{Qs} I_s}{S_{us}} \tag{13}$$

The number of turns N in the machine can also be calculated:

$$N = \frac{Z_{Qs} N_{slots}}{2m} \tag{14}$$

The motor will be 3-phase and 4-pole machine. The windings in the motor will be distributed throughout the stator slots as shown in Figure 14. As the efficiency of the motor is one of the most critical design aspects for this prototype, distributed windings have been chosen. For the best possible results, the windings will be manufactured and installed by a specialized company. The company will also install the epoxy, slot insulation and slot wedges for the windings.

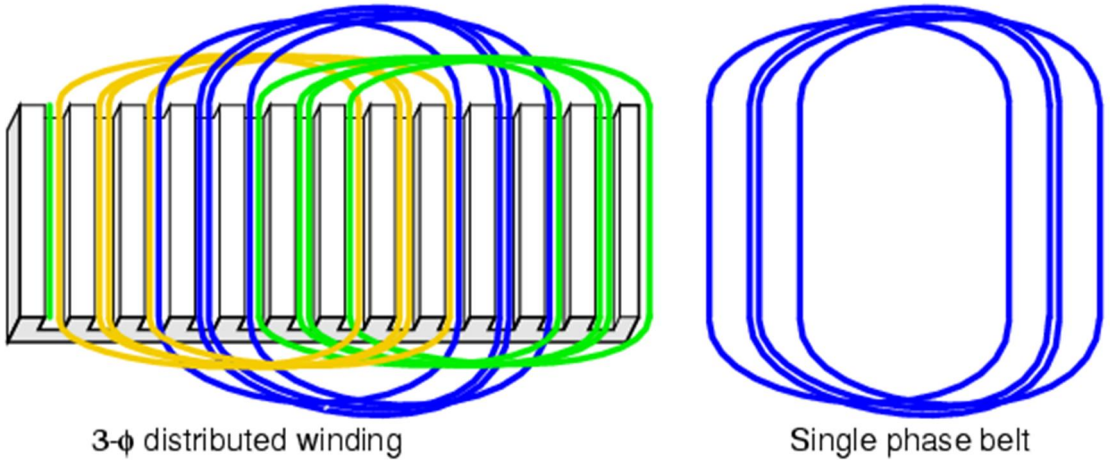

Figure 14: Example winding layout [32]

3.1.6 Bearings

Bearings are a central piece in the design of an electric motor. The bearings will provide extra strength and rigidity to the system. There are three bearings utilized for this design, two of which are located on the rotor shaft. The inner race of the bearings will be an interference fit with the rotor shaft. Moreover, one face of each bearing will be pushed against the larger diameter of the shaft, and will serve as a way to locate the proper x-axis positioning of the bearings. These two bearings are the most critical bearings in the design. Bearings two and three in Figure 15 are on the rotor shaft, and will help provide vibration dampening. Bearing one will be press fit onto the shaft of the planetary gear using an interference fit.

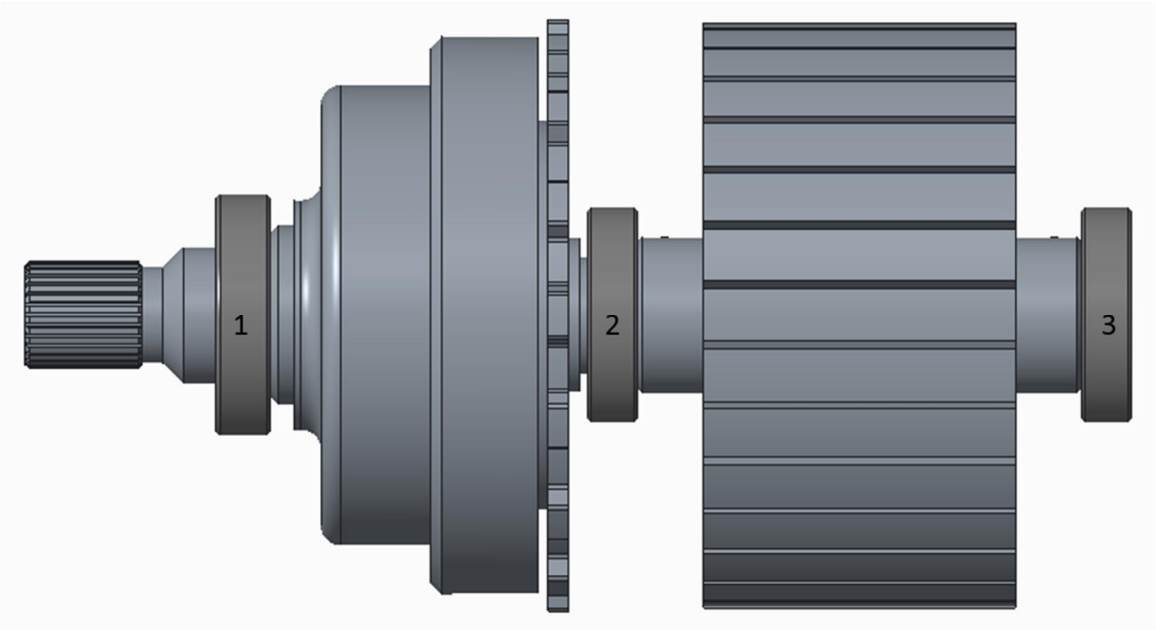

Figure 15: Bearing location. Planetary gear on the left and rotor on the right

These are deep groove ball bearings. Ball bearings provide low friction, minimal noise vibrations. These bearings are desirable for axial and radial load applications. However, for this application they will only be in radial loading. The bearings chosen for this application are ceramic bearings developed by *SKF*. They are specifically designed for electrical motors

and are resistant to electric currents, as the balls in the bearings are not made from steel or iron [33]. Furthermore, bearings two and three had to be capable of speeds up to 18,000 rpm, and have an inside diameter of 30 mm for the rotor shaft. *SKF* offers a 30 mm ceramic hybrid bearing that have a limiting speed of 19,000 rpm. Bearing one only needs to rotate at 6,000 rpm after the gear reduction. The planetary gear has a shaft size of 35 mm, so that was the bearing size chosen for bearing one. That ceramic bearing has a limiting speed of 17,000 rpm. This bearing will not be in direct contact with electrical currents; however, it was chosen to utilize the same type of bearings and to ensure that it would not be affected in any way. The outer diameter of bearings two and three is 55 mm, and of bearing one is 62 mm. These are the dimensions used in the frame components to encase the bearings. The bearings will use high-strength bearing locking adhesive to prevent the outer race from rotating in the housings. It will also provide sealing.

3.1.7 Frequency Converter

The converter will be sourced from *ABB*. It will provide 3-phase voltage between the range of 380 and 500 volts and an output frequency of up to 599 Hz. Many converters are available that meet the needs of this motor. For example, *ABB* machinery drive model number *ACS850* is a good example of a converter that will be capable of powering this machine. The specification sheet can be seen in [34]. Using pulse-width modulation voltage supply can reduce the low-order harmonics and improve efficiency with a coil pitch of 120 degrees [35].

3.1.8 Planetary Gear

Designing a planetary gear from scratch is not necessary; many companies make off the shelf planetary gears. Finding the correct planetary gear however, proved a difficult task. It was previously determined that there were some initial constraints to be met. Those constraints are listed below:

- Reduction ratio of 3 or similar
- Capable of an input speed of 18,000 rpm
- Nominal torque value of 60 Nm
- Dimensions are smaller or similar in size to the induction motor

Initially, it was believed that *Bosch Rexroth* had an off the shelf solution that would meet these requirements. After further research, that was not the case. The gears were for heavy-duty applications. They were too large and heavy for the needs of this project. Next, *Matex Gears* was found with some off the shelf solutions. It was determined that the gears with a reduction ratio of three had a maximum input speed of 5,000 rpm. The centrifugal forces on the sub-components were computed to determine how problematic rotating the gear system at higher speeds would be. The centrifugal force F is

$$F = \frac{mv^2}{r} \tag{15}$$

where m is the mass of the component, v is the velocity and r is the radius. Using a radius of 0.0325 m and 0.08 kg, the planetary gears were calculated to have a centrifugal force of 79.13 N with a rotating speed of 1,666 rpm after the speed reduction. When comparing this to the speeds that we require at 6,000 rpm, the centrifugal force was 1026.44 N. This is almost 13 times the rated force. This demonstrated that this gear train was not usable at those operating speeds.

Formerly, a few planetary gear trains from two *Toyota Prius'* were found. The gear sets were from a second and third generation *Prius*. This system proved to be difficult to use as the power input and output were on the same side of the gear train system as shown in Figure 16. The second-generation gears were larger and more robust. The gear set from the second generation was put on a lathe and some material was removed to try to remove the shaft from the planet carrier and turn it around. This would allow the input and output to be on opposite sides. The shaft was not designed to be removed, and if removed, the strength of the planetary gear train would be compromised. In addition, maintaining tight tolerances would be difficult if it was put back together. Detailed information about these gears were previously studied during another thesis [23], and provided insight on the operation of these planetary gears.

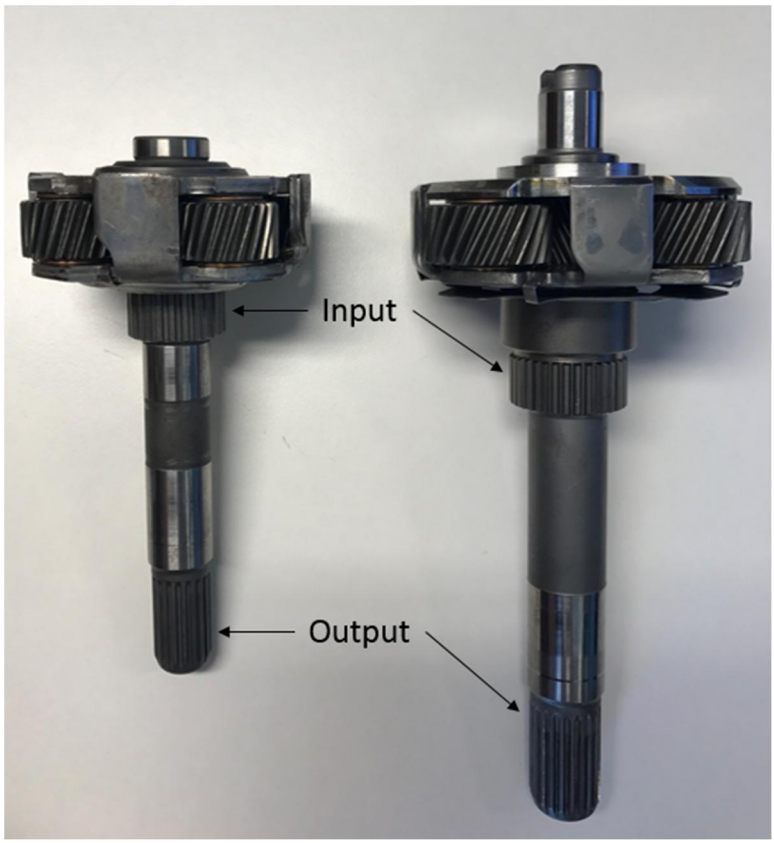

Figure 16: Prius planetary gears

After extensive research and communication with multiple parties, it seemed that the best option would to utilize a planetary gear from an automatic transmission. *ZF transmissions* makes many different planetary gears that seemed to meet the needs established. This company makes multiple transmissions for many car manufacturers. Typically, these transmissions were used in *BMW's* and *Audi's*. The focus was to find a broken transmission that someone would be willing to donate to the university. An old *BMW* transmission was found online. The owner was contacted and was willing to donate the transmission, as he had no use for it anymore. The transmission model number was *ZF 5HP18*. The planetary gears in this transmission had a few key qualities that made it a good candidate for the project. First, the input and output were on opposite sides, unlike the *Prius* planetary gear. Second, the front-end planetary gear had a high input speed from the ICE. Third, with the ring gear held stationary, it provided a gear ratio of 3:1. All of these were important

parameters that met the initial requirements. Further information about the transmission used can be found in [36].

After the transmission was acquired, it was dismantled piece by piece to access the front-end planetary gear located inside. The disassembly figures can be seen in Appendix 1. The first step was to remove the transmission oil pan. Next, the valve train system was then removed. After that was removed, the final bolts could be removed that kept one of the clutch pack housings in place. Bolts holding in the input shaft housing were then removed to pull out the shaft and first clutch pack system. The broken component of the transmission was found during this process, it was a housing for a clutch pack. All the remaining components were then pulled out from the transmission housing, including the planetary gears. After everything was removed, the two planetary gears were observed to determine the condition and operating principals. The planetary gear train used can be seen in Figure 17.

Figure 17: Planetary gear system. Input on the left, and output on the right

This system proved to be an ideal choice for the design. The planetary gear was then measured and 3D modeled using Creo Parametric 3.0. This allowed for modeling of the entire system so the interfaces and dimensions could be used for the rest of the design.

3.1.9 Frame

The section will describe the frame or housing used to encase all of the components in the system. A 3D model was made of the entire prototype using all of the previously developed design constraints and dimensions. The final prototype design is shown in section 4.2. A cylindrical design is the most practical and common design for use in the automotive industry. A bottom surface mounting design was made for tabletop testing and storage. Figure 18 shows this design. The next design is mounted using the face where the output shaft is located. For prototyping, the machine will be mounted using the cylindrical design

like the one seen in Figure 19. This shows how it can be mounted when used in a vehicle. The second design is the focus as it will be the most practical for use in an automobile.

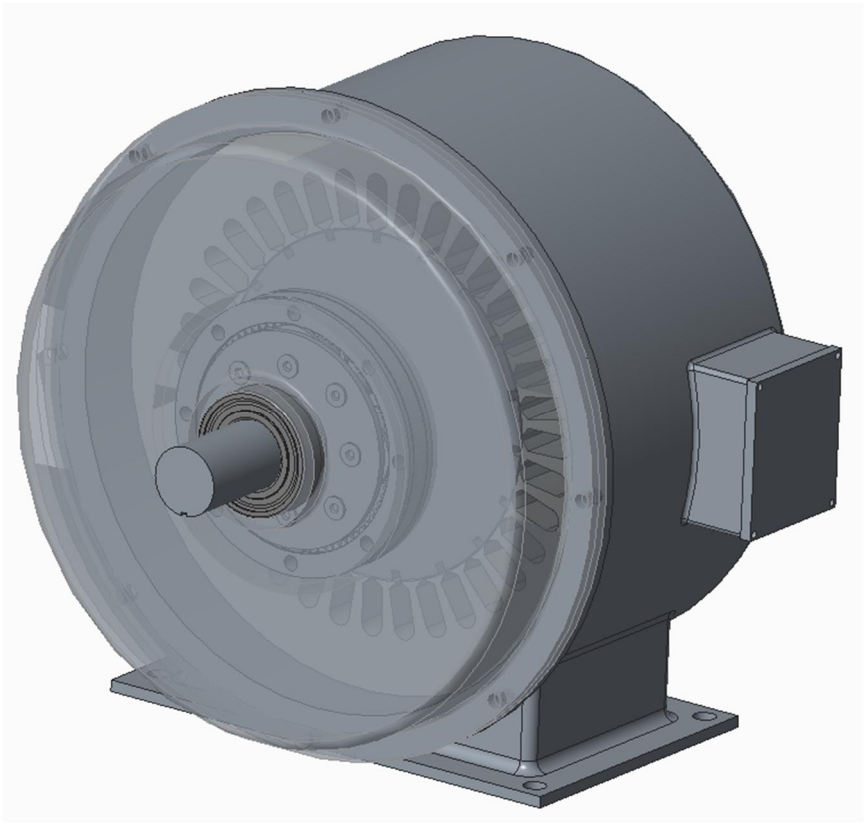

Figure 18: Bottom mounting design and entire prototype

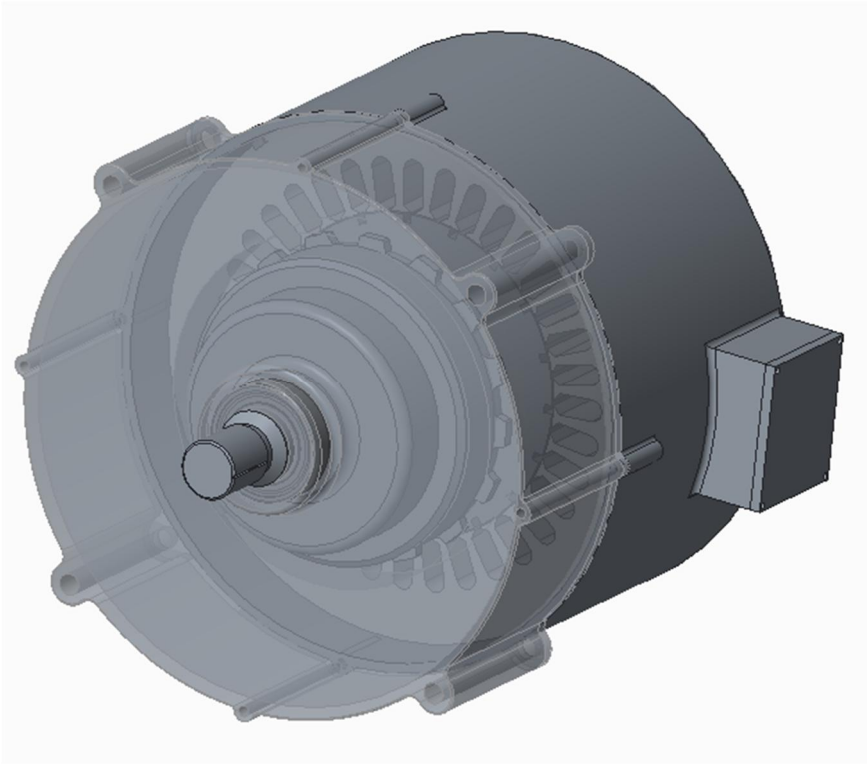

Figure 19: Cylindrical mounting design and entire prototype

Many iterations of the frame were designed; the figures above are early iterations, they are shown for displaying the different mounting configurations considered.

It is important that the entire frame can handle the speeds and vibrations that will occur. It needs to be rigid without adding too much mass. Thermally, it has to allow for airflow while the rotor is spinning to allow heat to escape. Oil channels are included in the design for proper cooling of the electric motor. After manufacturing, a suitable oil pump will be found with adequate oil pressure. With the addition of an oil pump, there should be an oil drain pan to collect all the oil so the pump can recirculate it into the system. This is not in the scope of this thesis.

The frame includes many different components. Each component and design decision will be explained. The main components include:

- Stator housing
- Stator guides
- Non-drive end housing
- Planetary gear support plate
- Drive-end housing
- Lifting hooks/feet

In addition, bolts, nuts, washers, spacers, bearing adhesive and gasket maker are used in the design. This design is made for the initial prototype testing, and changes may be necessary in the future, if unforeseen issues arise during manufacturing and testing.

The main component of the entire system is the stator housing. Everything will be bolted up or mounted to this component. This can be seen in Figure 20. Many items have been considered for the final design. On the front mounting face, there are twelve holes for securing this component with the other components. Those mounting holes are on a lip. This lip will allow adequate space so the bolt heads or nuts do not contact the rest of the housing. On the same face, there are four holes for disassembly. When the entire system is assembled, these holes can be used to thread in a bolt and push against the planetary support plate to separate them, as it could be difficult otherwise with the gasket used for sealing. Inside the stator housing is a small lip; this is used for when the stator is inserted. This will provide accurate depth placement. In addition, while inserting the stator, stator guides are used. The guides are used to prevent rotation upon installation, as seen in Figure 21. These guides are bolted into place with two holes each. The stator guides are 85 mm long with two mounting holes. The bottom face of the guide has a radius to match that of the stator housing inside diameter. The inserting procedure will require either the stator or the housing to be heated, and the opposite component to be cooled. After the stator has been properly installed, four holes are drilled in the side of the stator housing to provide additional securing points using bolts. At the bottom of the housing, are two large oil drain holes, one will be on each side of the stator, once it is installed. Another large hole is drilled on the side for the wiring to pass though and connect to the converter. A single small hole is also drilled on the side for a thermocouple wire to pass through and measure the temperature of the stator during operation. Six holes are drilled on the back face for the non-drive end housing to be bolted on. The non-drive end housing can be seen in Figure 22. Finally, on the outside of the housing is a strength lip, designed to provide additional support if needed to the design. If not needed, it can be machined off to provide mass savings.

All of the holes that do not have bolts placed in them during operation, such as the wiring hole and thermocouple hold will require sealing to prevent oil from escaping. The largest outside diameter of the housing is 290 mm, and the average wall thickness of the housing is 10 mm. The stator housing will be milled from a half-meter length of aluminum rod. Although the housing is only 140 mm long, additional length will be used for other components. In addition, additional length is required for mounting the rod in the machine used for the manufacturing process. Machining this out of a single piece of aluminum rod is not the most practical; however, the large size required warrants this. If multiple components were going to be made, casting would be the most effective way to manufacture this, but for prototyping, this is the most practical.

Figure 20: Stator housing

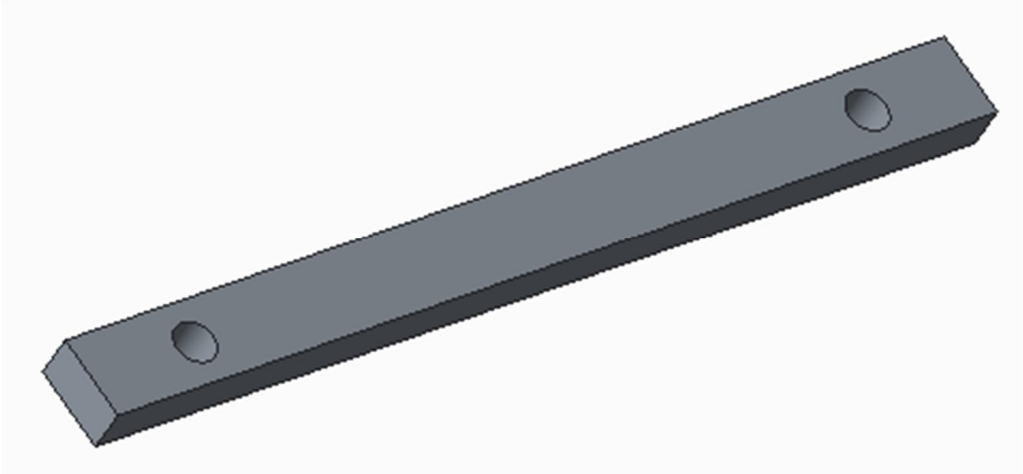

Figure 21: Stator guides

The non-drive end housing has an outside diameter of 270 mm to be flush with the back mounting face of the stator housing. There is a large ring on the back used to provide internal guidance and locating inside the stator housing. This allows this single design aspect to have accurate tolerances, instead of every mounting hole. The tolerances on the bearing mounting ring and larger ring are crucial for proper rotation of the rotor. Any improper tolerances in the rotor could cause wobble and unnecessary vibrations. Six oil cooling channels are drilled

though this ring for oil to be provided to the stator. The large center hole is also for oil cooling. It will provide oil to the planetary gear, through the rotor shaft. A single hose fitting can be seen in the center hole for the oil cooling line. The six other oil cooling holes will also require these fittings. The smaller ring on the inside will be the mounting location for one of the bearings. Six mounting holes and three disassembly holes are drilled in the end housing as well.

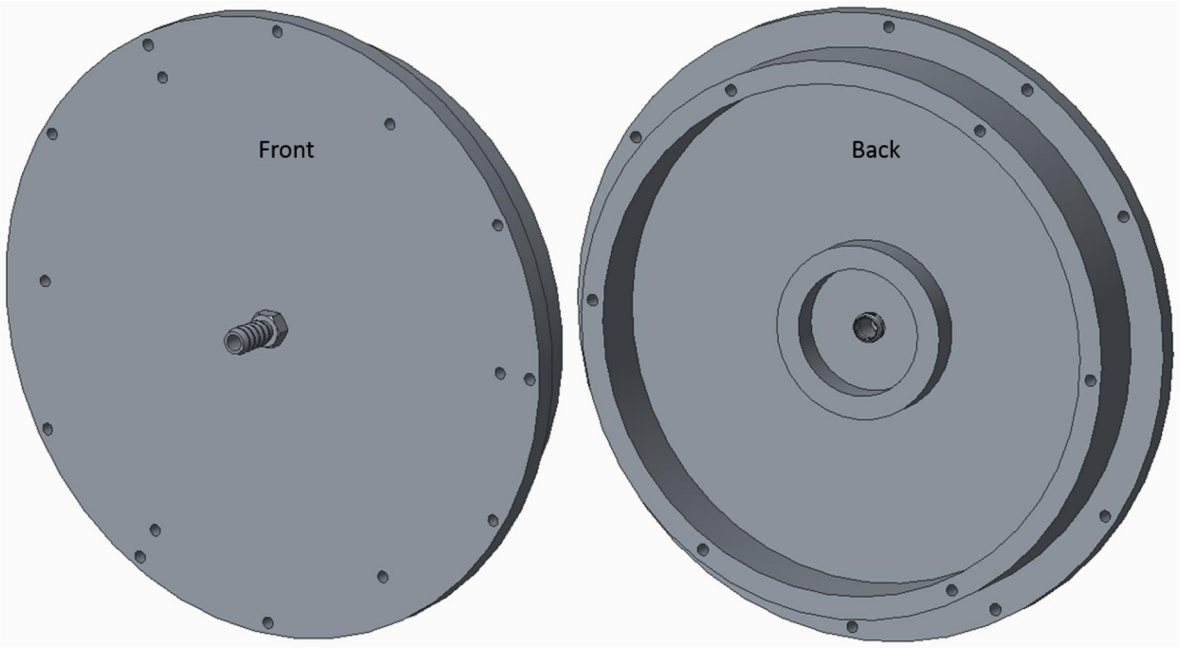

Figure 22: Non-drive end housing

The next design component is the planetary gear support plate, as seen in Figure 23. This component is placed in between the stator housing and the drive-end housing. On the front face is the placement ring for the ring gear of the planetary system. Once the planetary gear is installed, this will lock the ring gear in place and prevent it from rotating. Located on the front and back of the plate is a locating ring just like the non-drive end housing. It will allow proper alignment in the stator housing and the drive-end housing. In the center of the plate is a large hole for the rotor shaft to pass though and connect to the planetary gear. Twelve holes are drilled for mounting. These are pass-through holes. The mounting bolts will pass though the drive-end housing, the support plate, and the stator housing. Once the nuts are on, all three components will be squeezed together. At the bottom of the support plate is a hole for oil to flow and drain freely between the drive-end housing and the stator housing. The last part on the support plate is the bearing mounting ring on the back face. This is the same design as on the non-drive end housing.

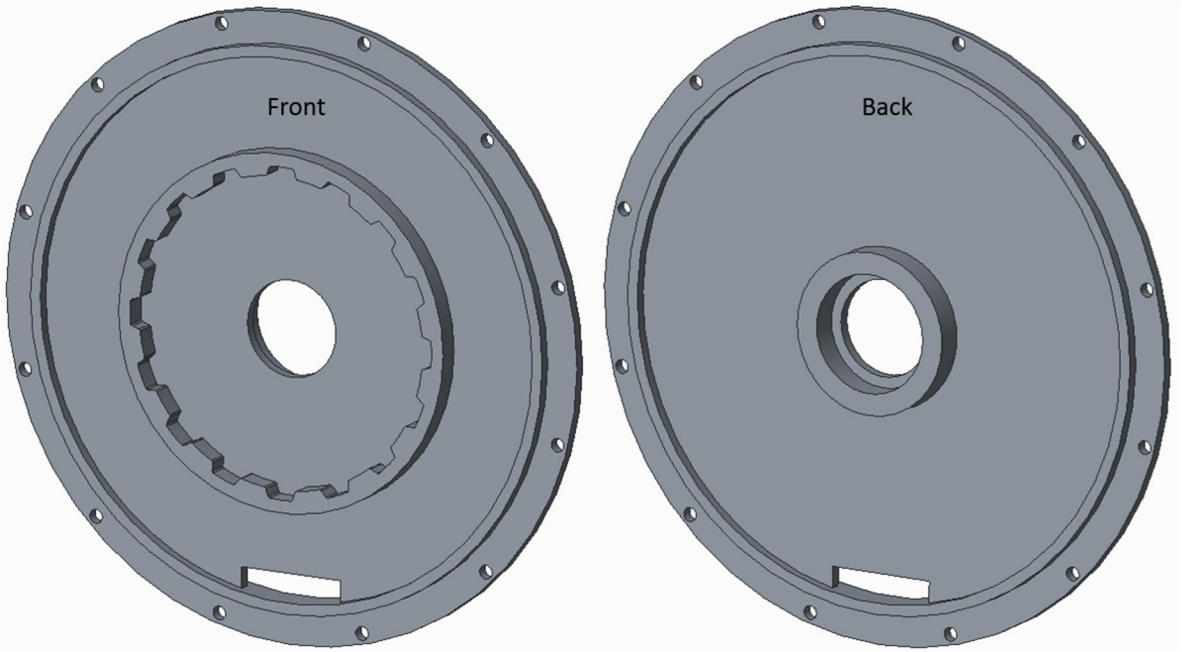

Figure 23: Planetary gear support plate

The drive-end housing is shown in Figure 24. This component has many similar features to the others, including four disassembly holes and twelve mounting holes. Inside the housing is a bearing mounting cutout, just as the other components. The drive-end housing has the same lip and diameter size of the stator housing. From the back view, it can be seen that the inside is hollow to allow room for the planetary gear. On the front view, there is an extruded feature that will allow the entire system to be mounted on a test bench. Multiple bolt patterns can be added for easy adaptability to other test benches. An oil drain hole is also included in the design.

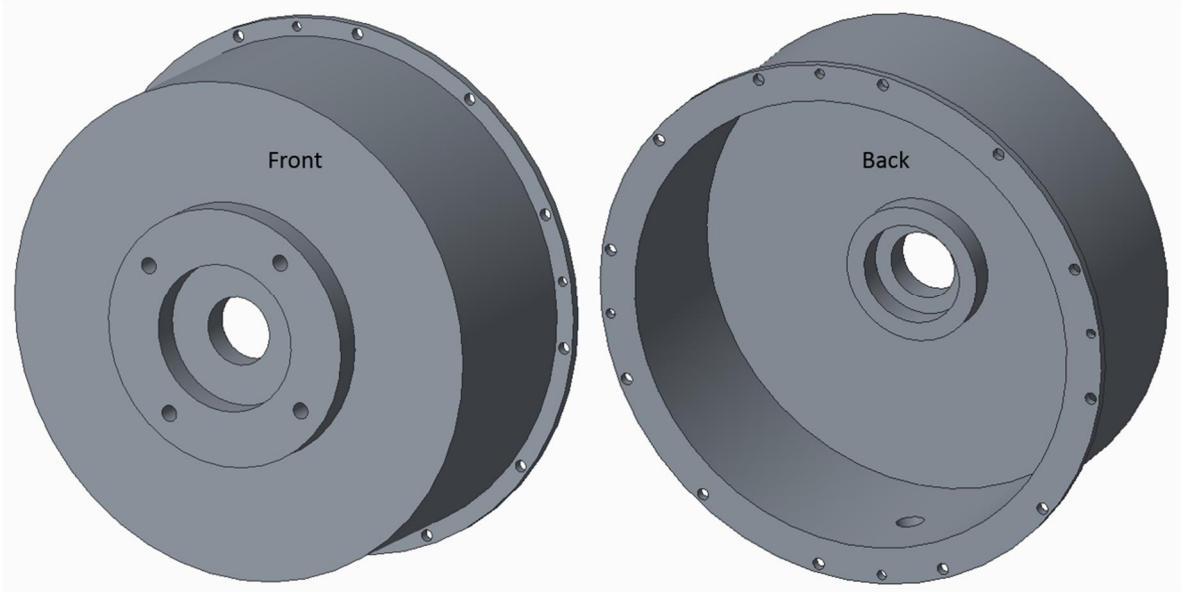

Figure 24: Drive-end housing

The drive-end housing can be removed without the support plate. However, the planetary gear would also have then be removed because the planetary gear will not be supported on

one end by the bearing located in the drive-end housing. This will cause a bending stress in the rotor shaft if it is not also removed. Once they are both removed, the bolts will then be reinserted through the stator housing and the support plate. When the support plate is removed, the rotor should be removed as well, because the rotor would not be supported on one side without the support plate. This will provide a way to inspect the stator.

A few features have been added for future use and testing. One of these is a bolt on hook for lifting the system with a crane. This hook bolts on through two of the existing mounting holes located on the drive-end housing. Figure 25 shows how this can be done. Multiple hooks can also be used to support the system on a table by acting as feet. However, another design for feet could be easily added by bolting it to the existing bolt patterns. In addition to the support hook, a hole is added for a thermocouple to measure the temperature of the stator during operation. Extra holes for additional thermocouples can be added easily. The next design consideration was the oil drain holes. In addition to the oil, these also allow air to escape. This allows moisture to escape which will prevent long-term corrosion.

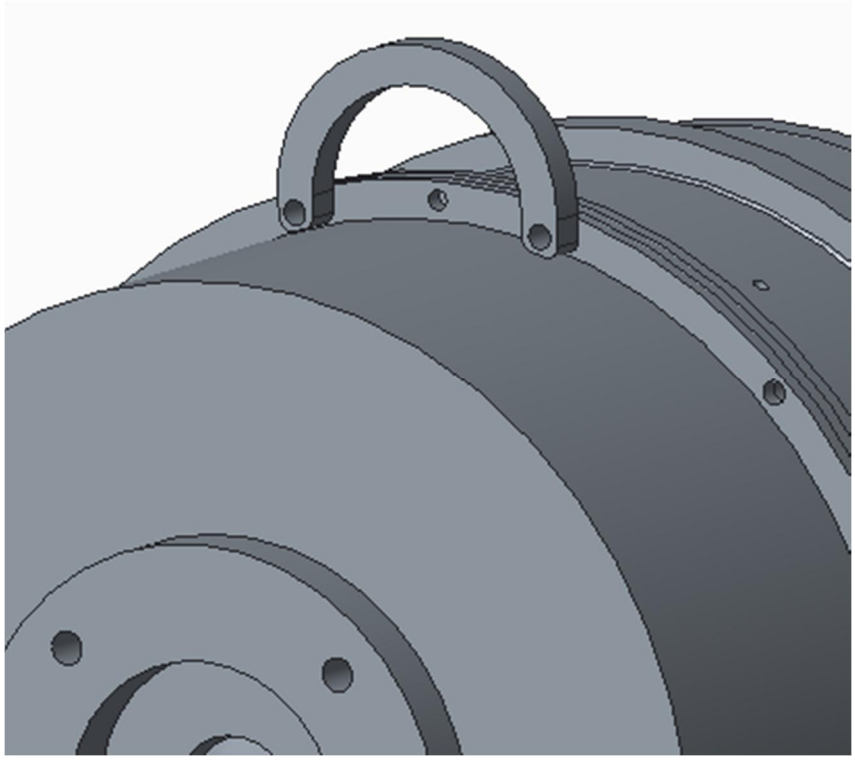

Figure 25: Lifting hook attached to the drive-end housing

It is important to note that the tolerances and fit for many of these components have not been exactly specified. When the product is being manufactured, the tolerances should be checked during the machining process to ensure the desired fit. All of the mounting faces will utilize a gasket maker compound or Room Temperature Vulcanization (RTV) silicon equivalent for sealing. It is easy to apply and easy to remove since the prototype will most likely be disassembled in the future for inspection or adding features. As previously stated, the bearings will use high-strength bearing locking adhesive.

3.2 Finite Element Method Simulations

There are many steps to creating a proper FEM simulation. This section is dedicated to the process required to perform these simulations. The objective of these simulations and the tools used to execute this will be explained. The steps used to analyze the results will also be described.

It is essential to have a plan on how to solve for the desired variables. Using FEM software with a computer provides a much faster solution for reaching the objective. The model can be modified to accommodate any needed changes with ease. This method is a huge time saver when compared to other methods such as trial and error of testing real prototypes.

The simulations are a continuation of the work completed by Jesse Mäntylä. The models were originally designed by him and were used for his work. They have been adapted to suit the needs of this project. Further information about Elmer and the programs used can be found in his thesis [7].

3.2.1 Software

The primary program used for the simulations was Elmer. Elmer is an open source finite element analysis program. Elmer consists of multiple programs to produce the final model and results. These include, ElmerGrid, ElmerGUI, ElmerSolver and ElmerPost. ElmerGrid is designed to make and change the mesh. ElmerGUI is the graphical user interface, or the actual program that lets you see the model. ElmerSolver is the portion that runs the code and mathematics for each individual element in the mesh. ElmerSolver is the most important software used for this project. ElmerPost can be used for analyzing the results from ElmerSolver. However, Paraview will be used instead of ElmerPost. Paraview is also an open source program that can turn data files into a visual representation. Matlab is also used for additional data processing. GMSH was used for making the geometry and the meshing required for ElmerSolver. Again, GMSH is an open source program.

The fact that Elmer is an open source program means that more problems and trouble areas are likely to happen. Elmer is developed by CSC – IT Center for Science in Finland. The open source publication was published in 2005, so Elmer is also a relatively new program. Many issues were found throughout this process, so using the most updated version of Elmer is vital.

The simulations were ran on a high performance computer, as the simulations require a lot of memory and processing power to complete. The average time to complete a simulation was eight hours.

3.2.2 Model Definition

Multiple design items went under the microscope during the process to finalize a design ready for prototyping. The first item that was studied in this thesis was the geometry of the stator slots using a current density supplied model. Next, the voltage, current and torque was tested using a voltage supplied model. The last item studied was the losses of the motor. The number of simulations required was quite high to reach the goal.

First, the model was setup using 2D simulations. This provided a simpler process to work with. The first set of simulations were to determine the best geometry of the stator slots. The number of stator slots, pole number and initial air gap were done previously. The air gap has

since changed, and the updated air gap is simulated in the later models. Each different geometry was ran through a simulation and the corresponding magnetic flux densities were analyzed. After all of the simulations were completed, the overall best geometry was decided.

The next set of simulations were done using the best geometry found. This step was to ensure that the voltages, currents and torque values of the induction motor are properly designed.

The last step is to verify the losses. The amount of losses is important from a thermal design aspect. The core losses or iron losses were analyzed. The losses will provide information about how efficient the motor is running, and how much energy is lost to heat.

3.2.3 Solving

The geometry was made using GMSH. Using the models from [7] as a starting point, GMSH can be used to create GEO files needed for meshing and ElmerSolver. The models allow different parameters of the stator and rotor to be changed with relative ease.

GMSH is also utilized to create the mesh file. The mesh density can be changed if needed. The meshing was done in 2D, as the rest of the simulations are setup for 2D. An example of a 2D mesh created with GMSH is shown in Figure 26. A solver input file or SIF file is also needed for ElmerSolver. The SIF file defines the types of solvers and settings needed for ElmerSolver. The SIF files also includes all of the parameters and material definitions of the motor such as the speed, slip, lengths, moment of inertia, resistances and inductances. The ElmerSolver manual was used to help define the SIF file properly [37]. There are many different uses for ElmerSolver. The types of solvers available and the solvers used in this thesis are explained in [38]. This explains all of the math and variables that can be solved with ElmerSolver. The main solver used for this project was *MagnetoDynamics2D,* the computation of magnetic fields in 2D. Multiple solvers were used in conjunction with this one to form the final model definition. Different sections of the model can be broken up into additional files, such as the rotor and stator slots, and the cage body. The parameters of the motor can also be broken up into a separate parameters file. A detailed example of how to create all these files and the process from start to end can be found in [39].

An example of a SIF file can be found in Appendix 2. This shows all of the different sections of the file. All the different sections and settings used for this thesis are shown. This is only the SIF file and does not include the rest of the files for the simulations. The other files needed are the rotor slots file, stator slots file, geometry file, B-H curve file, cage body file, and the cage definitions file.

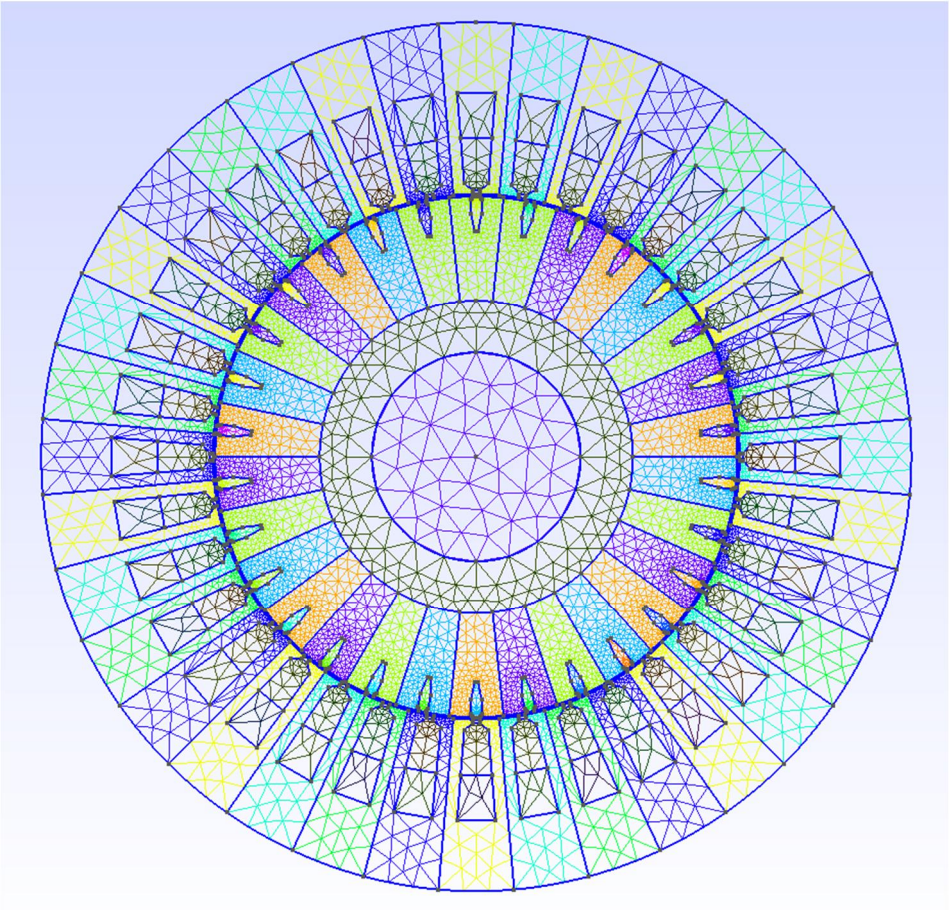

Figure 26: Geometry and mesh with 36 stator slots and 30 rotor bars

The B-H curve is the relationship of the magnetic field (H) and magnetic flux density (B) of a given material. The simulations require this file to define the electrical steel being used and the magnetic properties of the metal. It is simply a text document with two columns, of the B and H values corresponding to each other. Every material has a different B-H curve depending on the composition of the metal. The material is generally defined by the thickness of the sheets and the specific total loss at 1.5 T. Figure 27 shows three different B-H curve examples. 35PN230 would correspond to a sheet thickness of 0.35 mm and 230 W/kg specific total loss at 1.5 T. The material is also commonly written as M230-35A. The type of material used can have a huge impact on the performance of the machine. For example, when the silicon content increases, the core loss and saturation flux density decrease. A decrease in saturation flux density will result in an increase of copper losses [40].

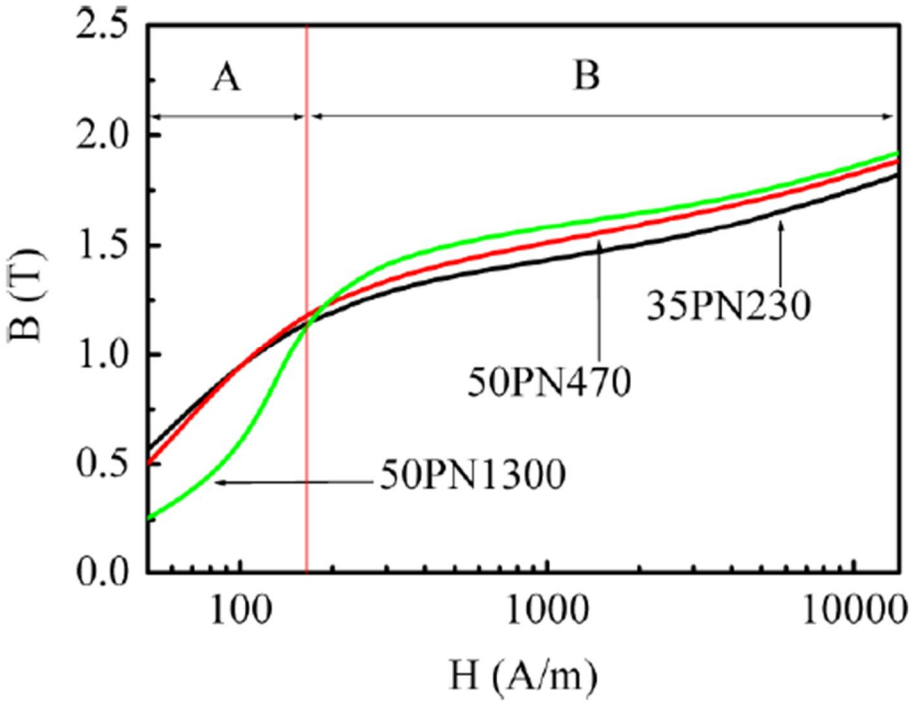

Figure 27: B-H curves of three common materials [40]

After everything previously mentioned is defined, ElmerSolver can then be run with all of the necessary files located in the same folder. ElmerSolver can be run from the ElmerGUI or it can be run from command line in windows and Linux. To help speed up the process an automatization program was created in [7], and is run in command line to create the mesh from the geometry, run ElmerGrid to get the meshing data for ElmerSolver, and start ElmerSolver. The results will then be published in the same folder for analysis. The simulations were done using a Linux operating system. The version of Linux was Ubuntu 14.04 LTS.

Any additional information desired about the files used and how to setup Elmer can be found in [7] and [37], and thus is not explained in more detail in this thesis.

3.2.4 Results Analysis

Matlab and Paraview are used for all of the post-processing. After the ElmerSolver has finished, the results are saved into a VTU file format. Paraview can use this file format. Matlab analysis was done with a DAT file that was also saved by ElmerSolver. The DAT file has many values in different columns. Each column corresponds to a specific variable. A file is also saved by ElmerSolver that shows what variable is in each column. Matlab was used to read the data and turn it into graphs. Matlab will be used to analyze the torque, voltage and current levels of the model. The output provided from Matlab will be a visual representation to assist with the results analysis. This will be the easiest way to determine exactly what is happening, and allow easy comparison to other results. Paraview will be used for analysis of the magnetic flux densities. The analysis in Paraview will be done by measuring the magnetic flux densities at multiple intersection points of the mesh.

4 Results

The results are broken up into three main sections. The simulations results, the final mechanical design from 3D modeling, and the cost. The geometry resulting from the electromagnetic FEM simulations are included in the 3D modeling. This provides the complete system design.

4.1 Electromagnetic Finite Element Analysis

The simulations done were completed in steps. The first step was to determine the best stator slot geometry using a current supplied model. Next, simulations using a voltage-supplied model were done. Finally, the losses of the final design were simulated. The results are compared to other electric machines and designs.

4.1.1 Design of Stator Slots and Conductors

The geometry of the stator slots are the focus of this section. This section is based on simulations setup in [7]. The simulations were setup using a current density supplied electric motor. The basic operation of the simulations were not changed from [7], the geometry and current densities were adjusted to determine the final geometry. For these simulations with Elmer, eight different solvers were used. These solvers were:

- FreeMotion
- RigidMeshMapper
- CircuitsAndDynamics
- MagnettoDynamics2D
- MagnettoDynamicsCalcFields
- CircuitsOutput
- ResultOutputSolver
- SaveData

The setup for the current supplied model can be seen in SIF file in Appendix 2. This shows all of the different input parameters used and how the solvers are used in the model. The model is ran using current supplied in the stator slots and a circuit for the rotor cage windings.

Over twenty different geometries were prepared for simulations. Fifteen geometries were analyzed in detail. Ten slots used an angled slot opening and five slots used a square slot opening. Information about these slots can be found in Table 1. Besides the shape, the main difference is the slot area. The slot areas ranged from 223 mm^2 to 400 mm^2. These areas were calculated from the geometry files used in the simulations. Examples of a few slot shapes can be seen in Figure 28. Every geometry had different sizes of the slots, teeth and yoke. Changing the geometry changes the number of conductors and current density. The actual number of conductors that would be used is shown as well, because the value needs to be an integer. The current density of each slot was calculated using equations (8) – (14). For these calculations, a value of 8.00 was used for J_s to provide the smallest conductor area possible at 17.32 mm^2.

Table 1: Slot geometry information

Slot Type	S_{us} [mm^2]	Z_{Qs}	Actual Z_{Qs}	J_{slot} [A/mm^2]
Angled 1	307	8.86	9	4.06
Angled 2	285	8.23	8	3.89
Angled 3	294	8.48	8	3.77
Angled 4	247	7.13	7	3.93
Angled 5	223	6.44	6	3.73
Angled 6	299	8.63	9	4.17
Angled 7	281	8.11	8	3.95
Angled 8	263	7.59	8	4.22
Angled 9	245	7.07	7	3.96
Angled 10	227	6.55	7	4.27
Square 1	244	7.04	7	3.98
Square 2	292	8.43	8	3.80
Square 3	344	9.93	10	4.03
Square 4	400	11.54	12	4.16
Square 5	460	13.28	13	3.92

Simulations were ran in Elmer to determine which shape was the overall best. First, every geometry was ran using the same parameters, and only the slot area was different. This let all the results be on a level playing field, so just the affect from the slot area could be analyzed. The results were analyzed by comparing the simulated magnetic flux densities. The magnetic flux density values received from the simulations were compared to theoretical maximum values for standard asynchronous machines listed in Table 2. The magnetic flux density values from the simulations can be seen in Table 3. For these simulations, the current density in all the slots was set to a value of 4.00 A/mm^2. This let the geometry be analyzed without any other influencing factors.

Table 2: Permitted flux densities for asynchronous machines. Adapted from [3]

Placement	B
Stator Yoke	1.4 - 1.7 T
Stator Teeth	1.4 - 2.1 T
Rotor Yoke	1.0 - 1.6 T
Rotor Teeth	1.5 - 2.2 T
Air Gap	0.7 - 0.9 T

Table 3: Magnetic flux densities from simulations

Slot Type	Stator		Rotor		Air Gap	Status
	Yoke	Teeth	Yoke	Teeth		
Angled 1	2.2 T	1.8 T	1.0 T	1.6 T	1.1 T	Bad
Angled 2	2.2 T	1.7 T	1.0 T	1.5 T	1.3 T	Bad
Angled 3	2.1 T	2.1 T	1.0 T	1.5 T	0.9 T	Good
Angled 4	2.0 T	2.1 T	1.0 T	1.7 T	1.1 T	OK
Angled 5	2.3 T	2.2 T	1.2 T	1.6 T	1.3 T	Bad
Angled 6	2.3 T	2.0 T	0.9 T	1.4 T	1.2 T	Bad
Angled 7	2.3 T	2.0 T	1.0 T	1.4 T	1.2 T	Bad
Angled 8	2.1 T	2.0 T	1.2 T	1.4 T	1.0 T	Bad
Angled 9	2.0 T	2.1 T	1.2 T	1.5 T	1.0 T	Good
Angled 10	2.0 T	2.1 T	1.2 T	1.8 T	1.1 T	OK
Square 1	2.0 T	2.1 T	1.0 T	1.5 T	1.1 T	Good
Square 2	2.1 T	2.0 T	0.9 T	1.4 T	1.0 T	Bad
Square 3	2.2 T	2.1 T	0.9 T	1.4 T	1.1 T	Bad
Square 4	2.2 T	2.1 T	0.8 T	1.3 T	0.9 T	Bad
Square 5	2.2 T	2.1 T	0.7 T	1.2 T	0.9 T	Bad

The three best geometries were chosen for further simulations. The three best were Angled 3, Angled 9, and Square 1 as seen in Figure 28. The actual current density was then calculated again using equations (8) – (14). The computed current density was then input into the simulations for further analysis of the magnetic flux densities and torque curves. The calculations were done using one parallel subconductor.

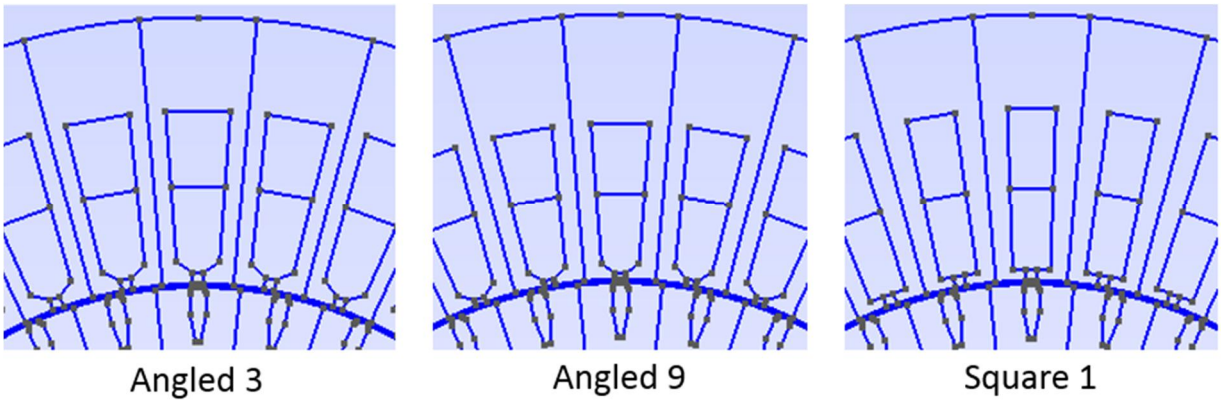

Figure 28: Three best stator slot geometries

The torque curves for the three best shapes can be seen in Figure 29, Figure 30 and Figure 31. All of the torque curves are similar. This was expected as the number of stator slots and the number of rotor bars affect the torque more than the slot shape. They all reach equilibrium around 0.1 seconds with a torque of 60 Nm. Since the torque curves were similar for all three geometries, the magnetic flux densities were analyzed to determine the overall best.

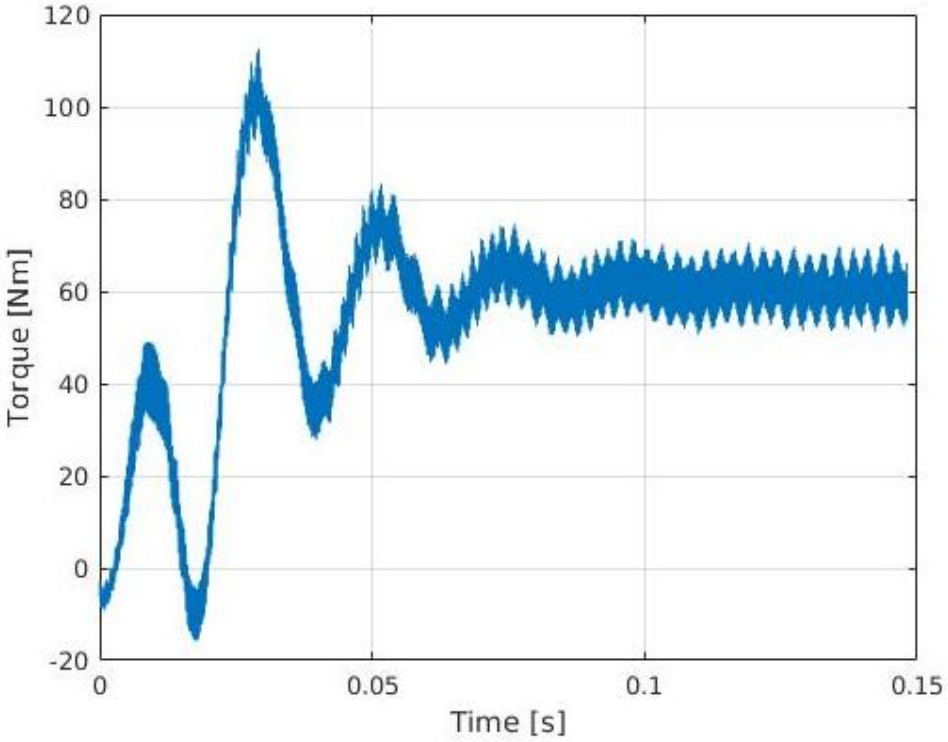

Figure 29: Torque curve for angled 3 geometry

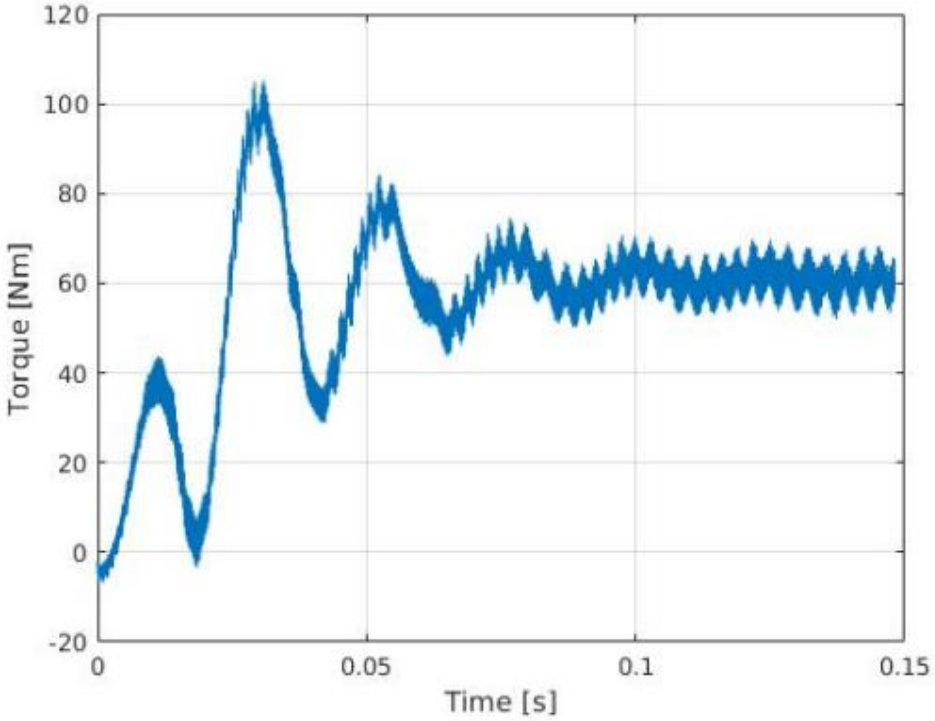

Figure 30: Torque curve for angled 9 geometry

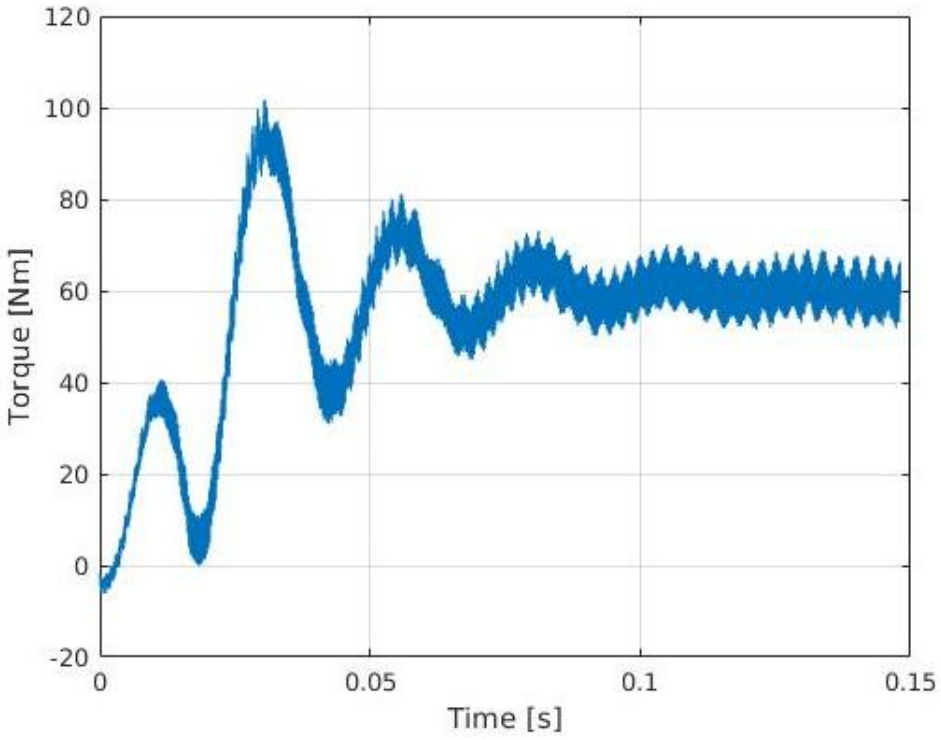

Figure 31: Torque curve for square 1 geometry

Angled 9 was the overall best geometry and can be seen in Figure 32. This shows that the maximum magnetic flux is 2.133 T. When taking a closer look, it can be seen that the extremely dark red is the only areas with that value. Only a few areas in the design have this value, and they are extremely concentrated. In real life, the values would be more evenly distributed. The values are at the intersections points of the mesh, so it cannot be as evenly distributed. Using a finer sized meshing could potentially help this a little. The actual calculated current density values and magnetic flux density values based on the corresponding geometries can be seen in Table 4.

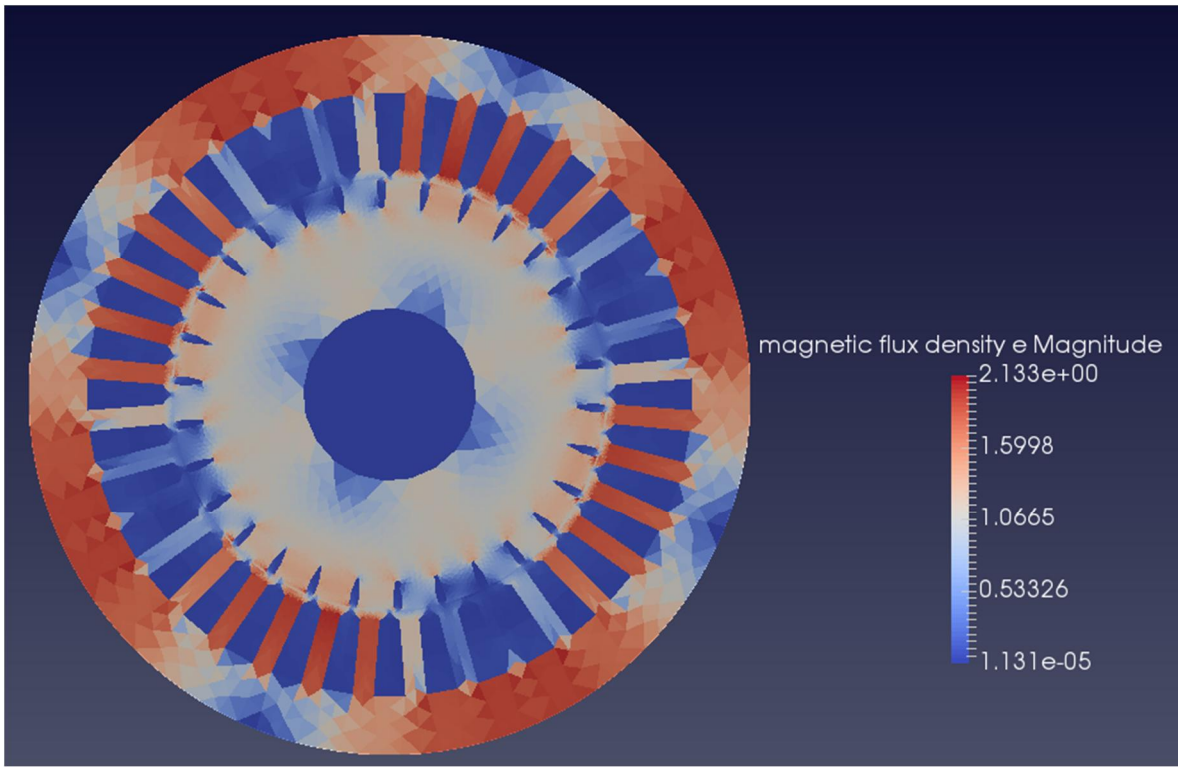

Figure 32: Angled 9 magnetic flux densities [T]

Table 4: Magnetic flux densities of the best slots with corrected current densities

Slot Type	J_{slot} [A/mm^2]	Stator		Rotor		Air Gap	Status
		Yoke	Teeth	Yoke	Teeth		
Angled 3	4.26	2.1 T	2.1 T	1.0 T	1.5 T	0.9 T	OK
Angled 9	3.96	2.0 T	2.1 T	1.2 T	1.5 T	0.9 T	Good
Square 1	3.98	2.0 T	2.1 T	1.0 T	1.5 T	1.1 T	OK

The results are the maxima values found. ParaView was used to determine the values at the intersection points of each of the mesh areas that were created during the process. The extreme outliers were not included because they were concentrated in one area and not distributed; this means that in real life, the flux density would be more evenly distributed throughout the entire stator yoke. The values given are the average maxima's. This gives a better approximation to real life scenarios.

If the values listed in Table 3 and Table 4 are higher than the allowed maxima's in Table 2 it was not of much concern, as the values were mostly concentrated to specific locations. This means that the average maxima would actually be lower.

These simulations were done with the original air gap of 0.7 mm and slot opening of 2.0 mm. After this step was completed, the design changed to the updated values that were determined from expert interviews and conferring with the companies who will manufacture the electric motor.

The material used for the B-H curve definition was M400-50A. This is the closest material definition found when compared to what is planned to be used. The planned material is M90-27A.

The simulations were done using a more advanced rotor design than what will be utilized for initial prototyping. The simulations use a squirrel cage rotor as it provides better magnetic characteristics. The rotor slots are using a copper material and the rest of the rotor is using the properties of the ferromagnetic iron M400-50A. However, this design is more complicated and costly. As stated before, the initial design is planned to be a solid slitted rotor without a squirrel cage for simplicity.

4.1.2 Voltage Supplied Simulations

This section was completed using a voltage suppled electric motor, instead of a current density supplied motor. These simulations are designed to provide a second means of verification that a proper design is ready for prototyping and manufacturing. The solvers used in Elmer are the same as the current density supplied model, minus the *FreeMotion* solver. The model is setup to use a circuit to simulate the stator and rotor windings. This model no longer uses a current density value for the stator slots. In addition, it no longer uses the moment of inertia, initial speed and initial angle for the rotor. However, the model does use the supply voltage as an input.

These simulations started with a 400 V star connected motor with the rotor and stator circuits implemented. The rotor is modelled at an imposed speed with a slip of 2%. The results received were not ideal; the torque and current values were too low. The reasoning for these low values is unsure. The torque value is negative because the rotor is rotating in the opposite direction as the previous simulations. The peak value of the phase voltage is around 320 volts. These simulations were done using Angled 9 geometry and the original air gap of 0.7 mm, slot opening of 2.0 mm, conductor area of 17.32 mm^2, and 8 conductors.

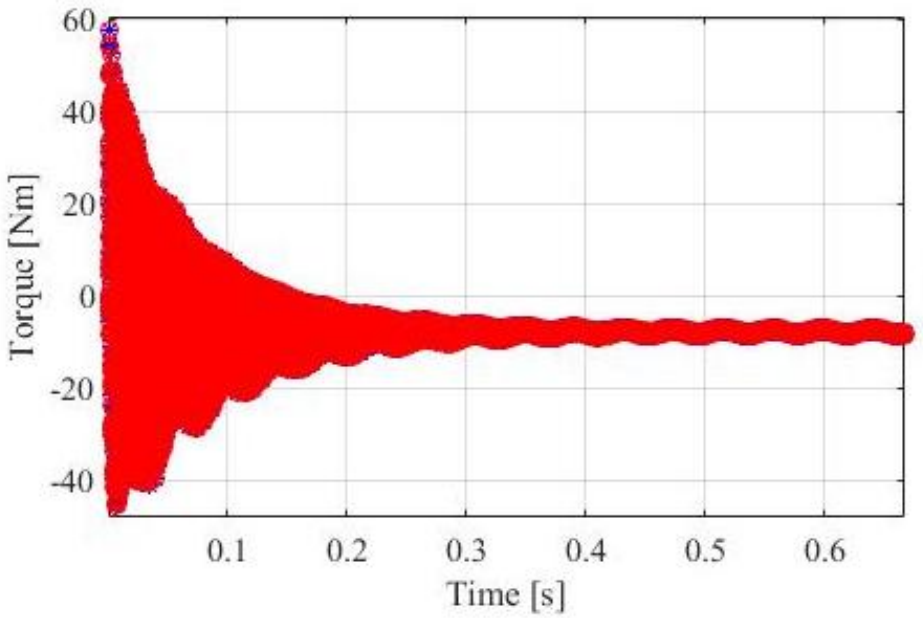

Figure 33: Torque level for 400 V star connected motor

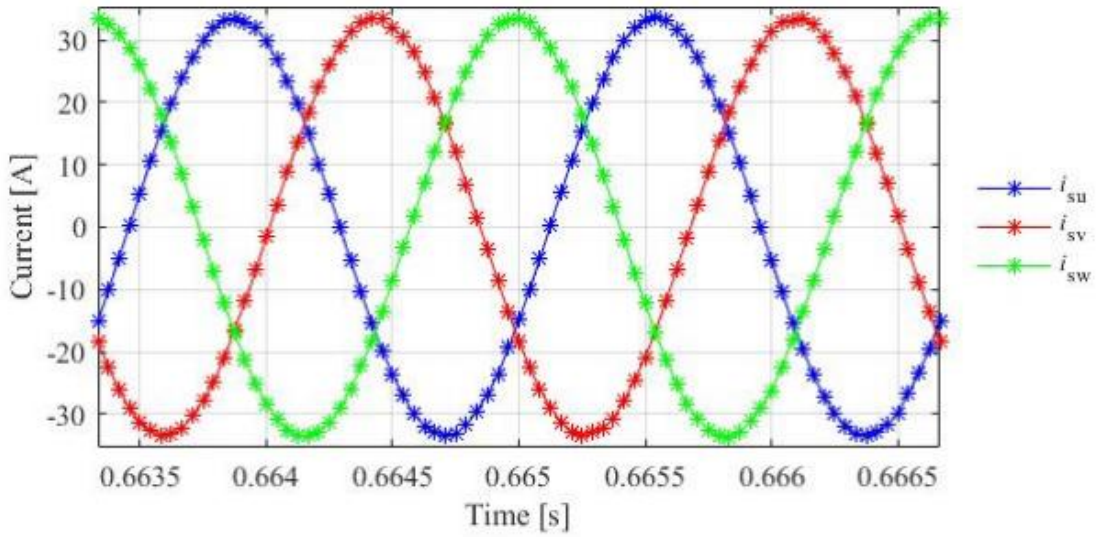

Figure 34: Current levels for 400 V star connected motor

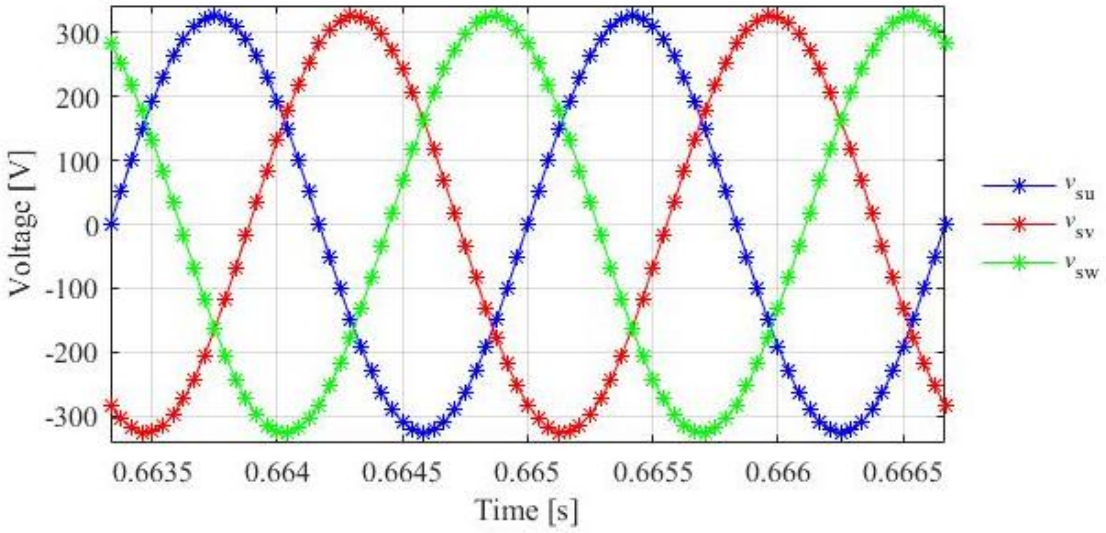

Figure 35: Voltage levels for 400 V star connected motor

Next, a simulation was started with an increased voltage of 500 volts; it also utilized the updated geometry that is used in section 4.1.3. Unfortunately, there were many issues with Elmer, so the voltage simulations could not be completed. At first, errors in the coding of Elmer were found. These errors were related to the physics of the program and produced unreliable results. This was fixed with an update of Elmer. Second, an issue with getting the model to converge was found when the voltage was increased to 500 volts for a star connected motor.

The process to define many of the parameters is an iterative process. Some of the values have to be specifically decided so that other values can be calculated. These parameters include the air gap, slot opening, space factor, phase current, and the conductor area or diameter.

The simulations are setup to run in parallel. This provides a sophisticated use of the cores in the central processing unit of the computer used. This takes a mesh and separates it into multiple parts. Each part can then be simulated on a specific core, and then it is reassembled once it is completed [37]. This was ran with the command './run.sh'. The convergence issue needs to be addressed first, and then the simulation needs to be properly ran with parallel computation.

4.1.3 Final Simulation and Losses

The final step was to analyze the losses in the final design chosen. This was also done with a current density supplied model, like in section 4.1.1. The losses will provide a better idea of how much energy is lost to heat. An additional solver was added to model called the *FourierLossSolver* to complete this step. This is shown in the SIF file in Appendix 2.

This design uses the final design with 3.5 mm air gap, 3.0 mm slot opening, and 0.6 mm wire diameter. This resulted in a current density of 4.53 A/mm^2. It is important that when using a wire diameter of this size, double layer winding should be used with parallel branches or paths. The final design and mesh is shown in Figure 36 using the Angled 9 geometry.

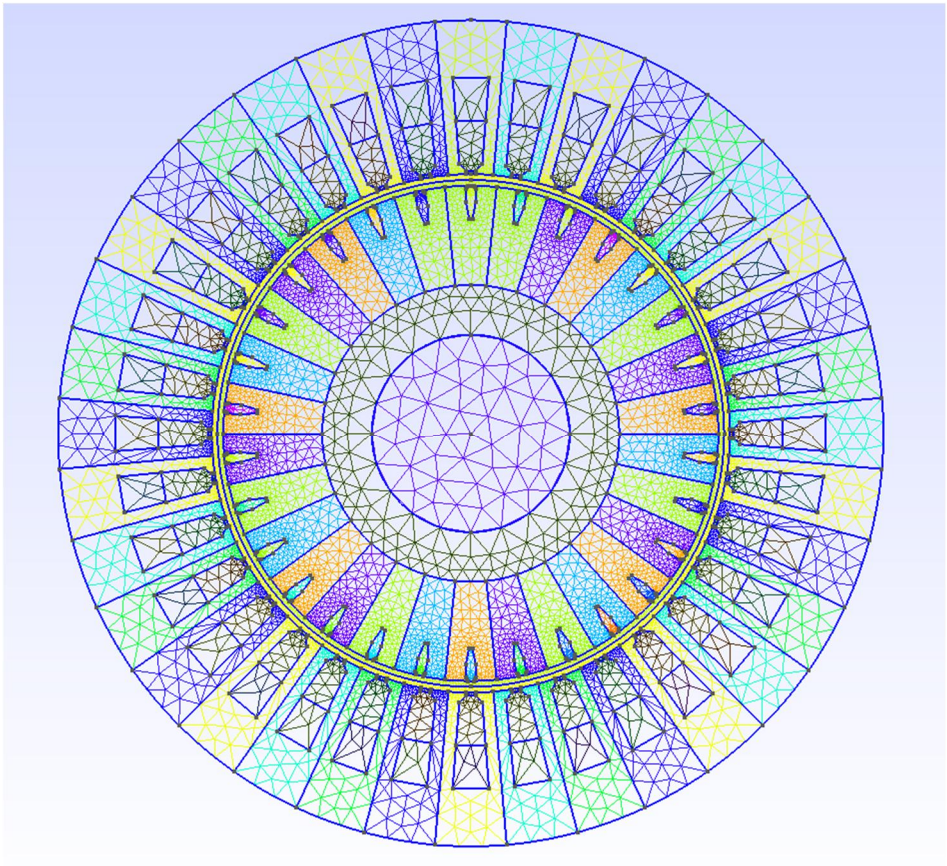

Figure 36: Final geometry design and mesh

The analysis was done just as in the previous section. The resulting magnetic flux densities are shown in Figure 37. The values are all within the permitted range from Table 2.

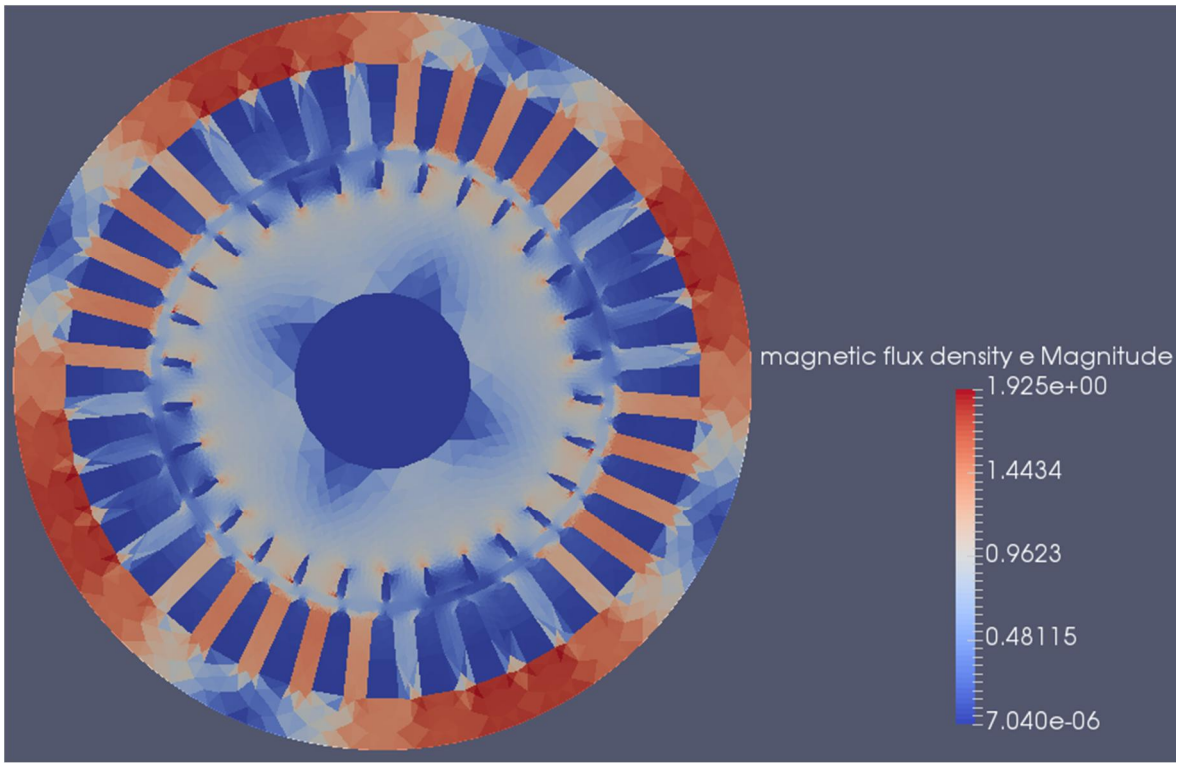

Figure 37: Final design magnetic flux densities [T]

The slip and toque of the design are shown in Figure 38 and Figure 39. The slip is about 1.1%. This value is in the acceptable range as the design is estimated for a slip of close to 2%. The torque reaches a steady value of 60 Nm. The curve is much smoother than the previous designs with a smaller air gap.

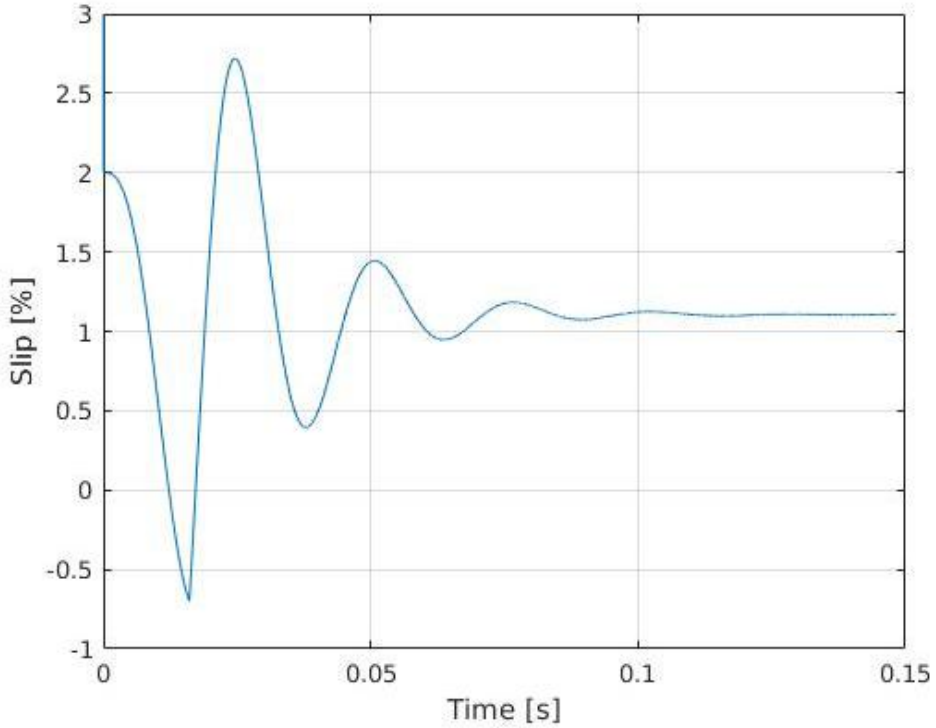

Figure 38: Percentage of slip of the final design

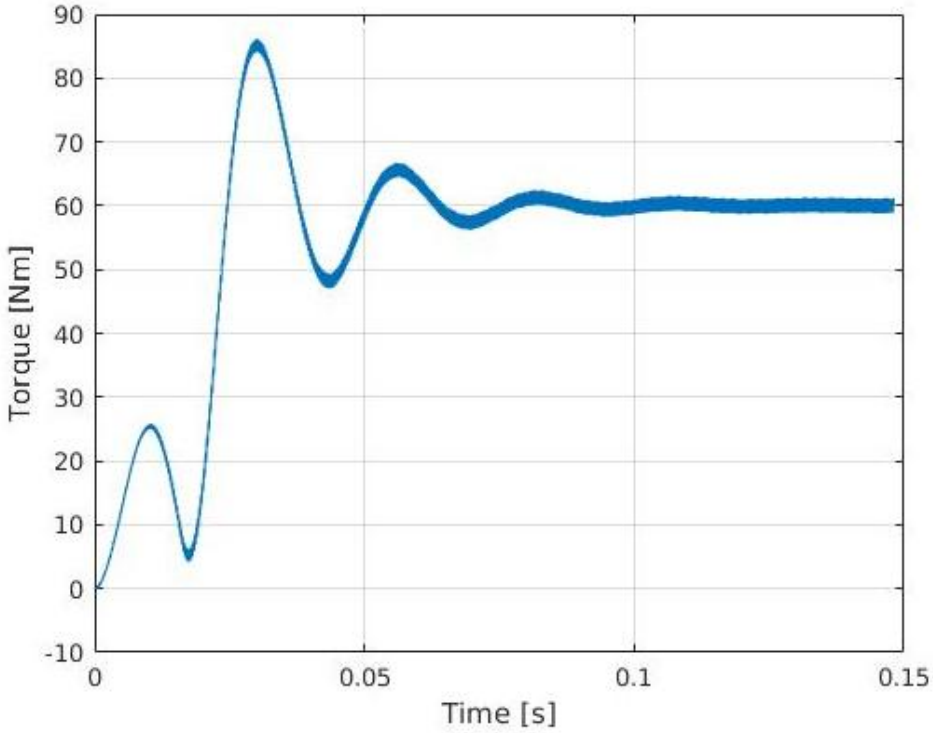

Figure 39: Torque curve of the final design

Table 5 shows the losses for the final design. These values are output from Elmer. Elmer outputs the values in watts per meter and have to be scaled to the length of the machine of 0.08 m. The total iron losses are the summation of the hysteresis losses and dynamic eddy current losses.

Table 5: Induction motor losses

Total hysteresis losses [kW]	0.98
Total dynamic eddy current losses [kW]	24.27

The total iron losses are 25.25 kW. The losses received are quite large. Using these values, the efficiency of the motor can be calculated. Equation 8 is used to determine the output power at 111.85 kW watts using a slip of 1.1% and a torque of 60 Nm. The efficiency is calculated using equation 3, taking the power output divided by the power input. The input power is summation of the output power and the losses, 137.10 kW. This provides an efficiency value of 82%. These results show that the motor is not as efficient when compared to other induction motors. Most induction motors have an efficiency value from 85-97%. The losses need to be reduced to improve the efficiency of the motor. The efficiency was previously estimated at 95% in section 3.1.5.

The iron losses received from Elmer are dependent upon coefficients that are predetermined and used in the SIF file. The coefficients used are estimates, and are the best available at this time.

4.1.4 Comparisons and Analysis

The overall design originated from the work done in [7]. Aspects of the design have changed to provide improvements and manufacturability. Both designs utilize a four pole, radial flux high-speed induction motor. The size of the stator slots, the air gap, the conductor diameter, the slot opening and the current density in the slots have all changed. The rotor and stator outer diameters, the number of stator slots, length of the machine, the number of rotor bars, and the rotor bar shape remained the same. Other characteristics such as, lamination sheets size, number of conductors, number of turns and space factor are now finalized.

When comparing this design to the *Chevrolet Bolt EV* [25], similarities are seen. This design uses a speed of 6,000 rpm and the *Bolt* uses 4,500 to 8,810 rpm. The size of the two motors are comparable, with a length of 125 mm, and outer diameter of around 200 mm for the *Bolt.* The *Bolt* has a peak torque of 360 Nm and maximum battery power of 150 kW. The peak torque for the final design in this thesis is around 90 Nm, and the shaft power is 112 kW. The *Bolt* achieves 97% efficiency. With an efficiency value of 82%, the design for this project needs improvement. Designing an electric motor with a high efficiency takes practice and care. Although, the efficiency value is lower than desired, the design is quite far along, but still has room for improvement.

The losses of a high-speed machine at 520Hz and 218kW are shown in Table 6 [41]. The total losses for the design presented in thesis is 25.25 kW. The 520 Hz motor has 32.26 kW of losses. The losses were analyzed in more detail for the 520 Hz motor. Total amount of losses is higher, but the power of the motor is also higher. In addition, the electric, friction, cooling and bearing losses were computed. Direct comparison is challenging, but the total losses in the stator and rotor for the 520 Hz motor is 7.66 kW. The design presented in this thesis has 25.25 kW of losses. This does not include the other types of losses such as fiction losses and cooling losses. The amount of dynamic eddy current losses for this project is large.

Table 6: Calculated losses for a high-speed 520Hz electric motor. Adapted from [41]

Electric Losses [kW]	7.7
Friction losses [kW]	4.6
Cooling losses [kW]	11.6
Bearing losses [kW]	0.7
Total stator losses [kW]	4.50
Total rotor losses [kW]	3.16

The losses presented in Table 7 correspond to a 120 kW synchronous electric generator [42]. They are used for comparison to a different type of machine with similar features. The design uses a star connected generator with a diameter of 430 mm and 1.2 mm air gap. Eddy current losses are much lower in the generator, again leading to the conclusion that the losses received for this thesis are higher than desired. The frequency in this design is much lower at 50 Hz, and the frequency affects the losses of the machine greatly. This is used to show how the losses of a lower speed and frequency machine compare.

Table 7: 2D Losses in a 50 Hz generator [42]

Loss Type	**Area**	**Value** [W]
Resistive Loss	Stator Winding	307.66
	Damping Cage	68.40
	Rotor Winding	411.83
	Other Conducting Part	141.68
Hysteresis Loss	Stator	618.24
	Rotor	148.25
Eddy Current Loss	Stator	403.45
	Rotor	1894.16
Excess Loss	Stator	187.80
	Rotor	101.85

Lamination thickness plays an important role on the amount of losses. Table 8 presents the rotor eddy current losses for the same generator. As the lamination thickness decreases, so does the eddy current losses.

Table 8: Rotor eddy current losses based on lamination sheet thickness [36]

Lamination Thickness [mm]	**Rotor eddy current loss** [W]
0.20	43.6
0.35	113.92
0.50	207.59
0.65	316.69
1.00	635.48
2.00	1894.16

The thickness used for the simulations in section 4.1.1 to 4.1.3 was 0.50 mm. The thickness of the material is simulated by using the correct B-H curve corresponding to the material. The desired lamination thickness is 0.27 mm. The correct B-H curve should be found and applied to the simulations. This will reduce the amount of eddy current losses in the machine, as the thickness of the material is almost being cut in half.

4.2 Final Design

This section provides the first look at the final design and the specifications of the motor. Figure 40 shows what the prototype will look like. To show how the components are assembled inside of the housing, Figure 41 shows a transparent view. Everything is assembled using a coincident axis in the center. Hardware and the oil fittings for the stator cooling lines are not included in the figures.

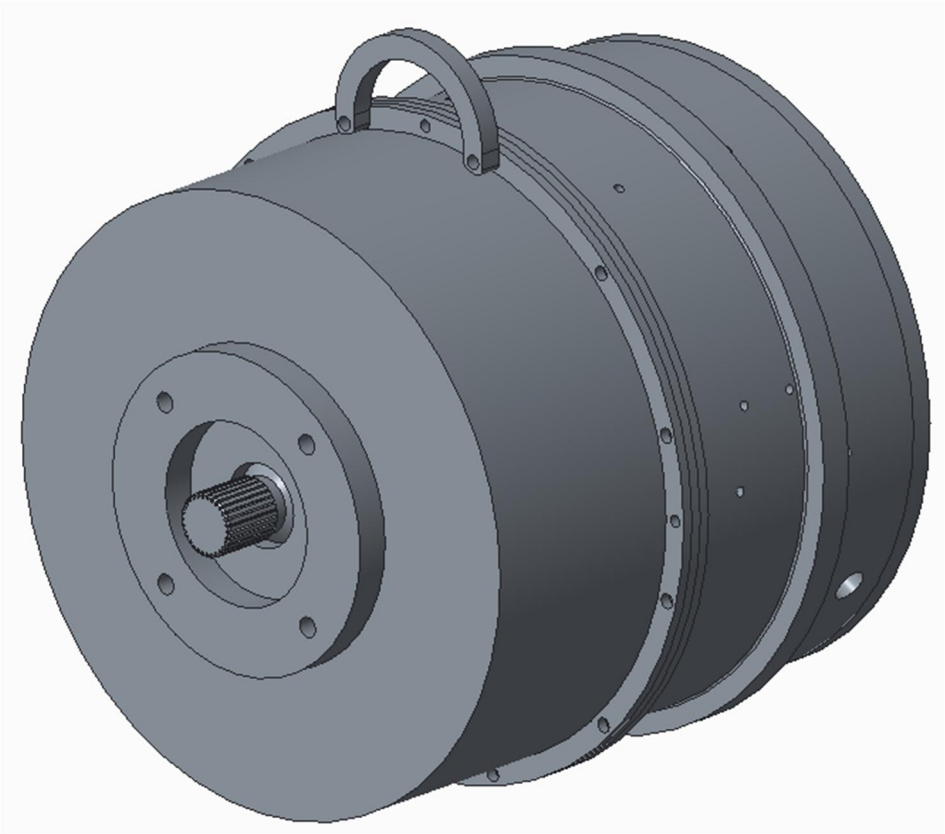

Figure 40: Final prototype design

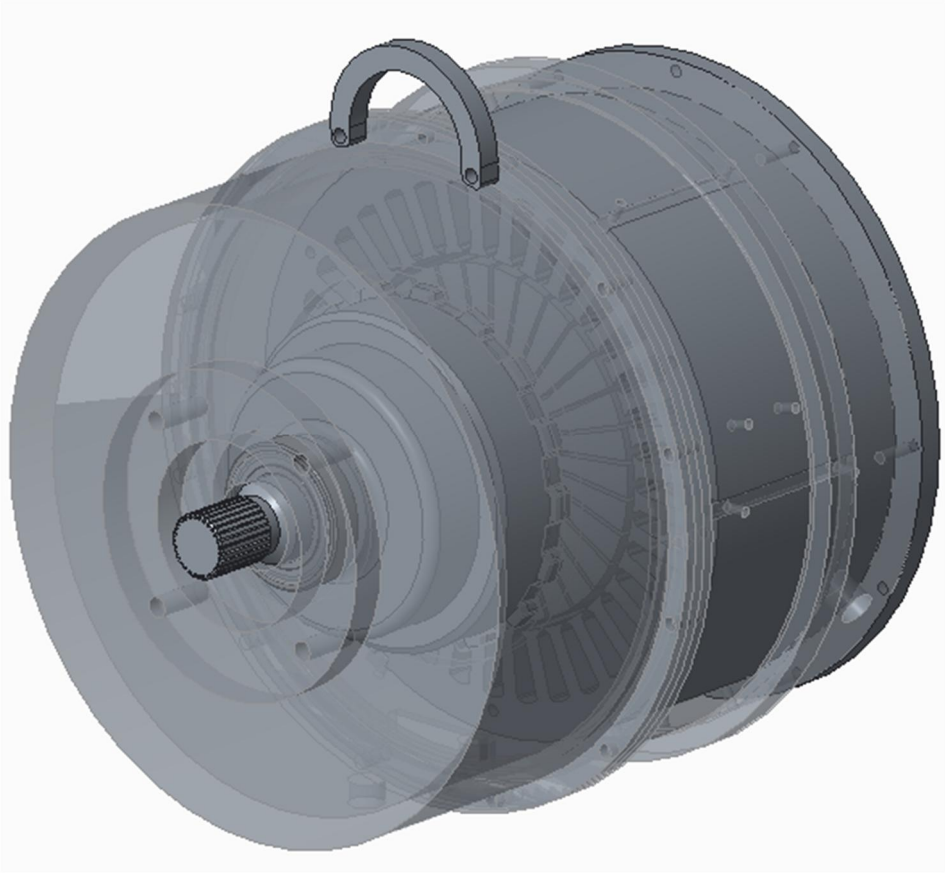

Figure 41: Transparent prototype design

This motor is planned to be Class A or Class B. This design uses normal starting torque with normal to low starting current and low slip. These are the most common classes for induction motors. The oil planned for the motor is polyester CC1105.

The lamination sheets for the stator are sourced from *Veslatec*. The thickness of the electrical steel will be 0.27 mm. The updated design will be used with the new air gap of 3.5 mm, 3.0 mm slot opening and 0.6 mm conductor diameter. The final specifications of the electric motor design is laid out in Table 9. The values used in the table are a combination of the calculated values and simulated values. The torque is the value received from the simulations, and the power is calculated using equation 8. A slip value of 1.1% was used, that was received from the simulations. This table shows all of the information that can be provided to the manufacturer along with a drawing file of the stator. A drawing file is provided in Appendix 3.

Table 9: Final high-speed induction motor specifications

Parameter	Value
Machine type	Induction machine – Radial flux
Number of phases	3
The number of poles	4 (2 pole pairs)
Number of stator slots	36
Maximum rotational speed	18,000 rpm
Maximum rotational speed after gear	6,000 rpm
Rotor type	Solid
Slip	1.1%
Torque	60 Nm
Rated frequency	600 Hz
Rated power	150 kW
Shaft power	112 kW
Stator current	136 Amps
Voltage	500 Volts
Phase voltage	289 Volts
Tangential stress	21500 Pa
Outer diameter of the stator	250 mm
Length of the machine	80 mm
Diameter of the rotor	150 mm
Air-gap length	3.5 mm
Stator slot height	~30 mm
Stator slot width	~10 mm
Stator slot opening	3.0 mm
Stator yoke thickness	~19 mm
Winding layout	Double-layer and distributed
Number of turns	48
Number of conductors per slot	8
Conductor diameter	0.6 mm
Space factor	0.5 – 0.6
Lamination thickness	0.27 mm

4.3 Bill of Materials and Cost

All the components required to manufacture the prototype are listed below. A detailed breakdown including the item, cost, manufacturer, and product number can be found in Table 10. The prices used are not final prices as nothing has been ordered. Estimates are entered for prices that are not known for items like the converter, stator windings, and rotor iron. Some quotes were provided by a few companies and have exact pricing.

Table 10: Bill of materials used for the prototype design

#	Item	Price (€)	Company	Product Number
1	Aluminum Rod	300	Alumeco	Aluminum Rod 300mmx600mm
2	35mm Bearing	30	SKF	6007-2RZTN9/HC5C3WT
3	Planetary Gear	0	N/A	N/A
4	Aluminum Plate	0	Aalto University	N/A
5	30mm Bearings	30	SKF	6006-2RZTN9/HC5C3WT
6	Rotor/Shaft Iron	150	Unknown	N/A
7	Stator Laminations	3,022	Veslatec	N/A
8	Stator Windings	1,000	Unknown	N/A
N/A	Hardware	0	Aalto University	N/A
N/A	Converter	500	ABB	ACS850
N/A	Bearing Glue	15	Würth	893603050
N/A	Oil	100	Stenbacka	Polyester CC1105
	Total	**5,147€**		

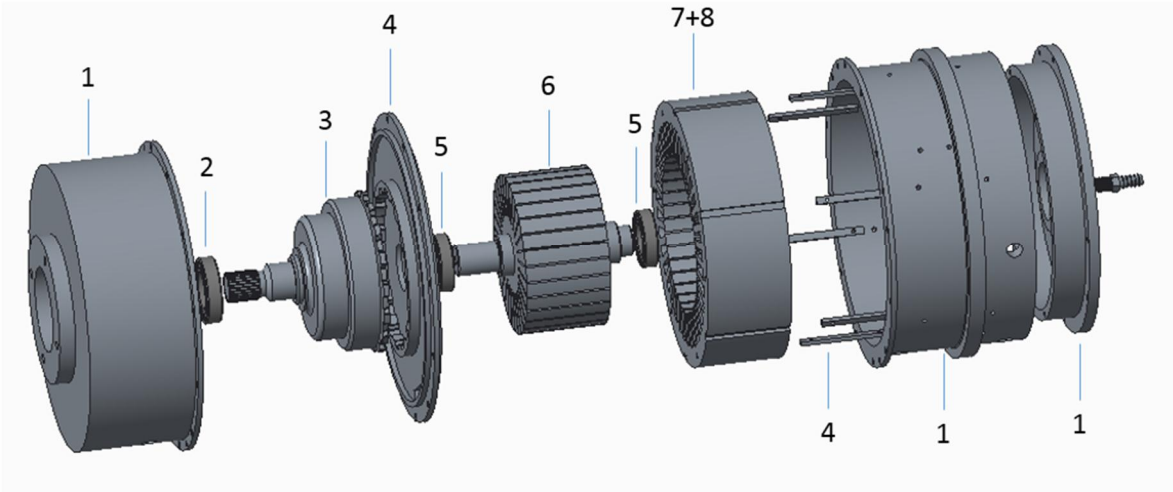

Figure 42: Exploded view of the prototype

Some of these items are already in possession of Aalto University or were donated for this project. Therefore, they were given a value of zero. The corresponding BOM items can be seen in Figure 42. Item four will be used to manufacture the planetary support plate and the stator guides. Item one is used for manufacturing the stator housing and the end housings. Item eight is the stator windings, which are distributed throughout the stator slots, and are not displayed in the figure. The hardware, converter, glue and oil is not pictured.

A specific goal was not set for the price of this project. The final price at 5,147€ is reasonable for an initial prototype.

5 Discussion

The design of the entire prototype has been described in detail. A few final simulations are required, and then the project should be ready for the next step, manufacturing. Manufacturing the prototype was the original plan for this thesis, but with unforeseen time issues and the vast amount of simulations needed, it was not possible. This section is designed to provide more insight to the work that went on during this thesis and the items that can be done in the future. The mechanical design, basic rotor dynamics, electromagnetic simulations, and iron losses have all be covered to determine the ideal geometry and setup.

5.1 Problems

During this thesis, some issues were found with the use of Elmer. Primarily, it is not a user-friendly program to use. The simulations can be ran from ElmerGUI, but for this project, everything was done using Terminal on Linux. Command Prompt for Windows operating systems can also be used. There is a bit of a learning curve to using the program, but is manageable with help from experienced users and the internet. Problems with the actual code of Elmer were found in addition to the model convergence issues discussed in section 4.1.3. Executing all the simulations with the tool given, required a significantly large effort. Some problems were found late in the work, and cost valuable time. Updating to the most current code solved some issues.

After some deliberation, it was decided that more work needed to be accomplished in regards to the design of the electric motor. The simulations completed were strictly focused on the induction motor, and mainly the stator. The rotor design was not developed extensively because a solid rotor should be sufficient for the initial testing. Again, this took an extensive amount of time, and a lot more than initially planned. Completing more detailed simulations with voltages and losses were done as well, since learning how to use Elmer had already been done. This validated the current design even further and provided more data to ensure the motor would be capable of the desired tasks. This thesis developed into furthering the design of the motor and completing the mechanical design of the entire system.

A lot of time was spent finding a suitable planetary gear. As previously discussed, multiple options were considered. No perfect solution was found. With time running out, the best option at the time was chosen. This ended up being the planetary gear from the *BMW*.

Doing the work on Linux also had a learning curve because some programs were setup differently than on Windows. This caused issues with Elmer trying to access the rights and files needed to run program. An intensive goal was set for this project, with finishing the design, simulations, and manufacturing the prototype. A more realistic goal should have been set and the simulation models should have been started sooner in the project. The design was believed to be further along and little to no simulations were planned, but that was not the case.

5.2 Future Development

One of the most important issues to study next is the structural design of the prototype. This includes both the design of the induction motor and mechanical design that houses the motor and planetary gear. Although the current design has been made to provide excess strength, thorough analysis has not been completed. The strength of the system is not of great concern, as it is over designed for this purpose. This is ideal for prototyping because any weak points

could be catastrophic under load. On the other hand, the added material, adds additional mass and cost. Extra mass can be a disadvantage when considering the fact that this is designed for automobiles. A heavier design means the system has to work hard and more energy will be required for movement. Weight savings is a key aspect to consider in automobile design. In the testing phase, the system will not be used in an actual automobile, so the mass is not so critical. After enough testing has be done, another design should be done to improve on the mass and other flaws found. For example, the wall thickness can be reduced, the support plate can be made thinner, or even different material choices for the housings. The current design is made from billet aluminum, which is light, but a final design will most likely be made from cast aluminum. This means that more intricate shapes could be implemented for weight and cost savings. Rigidity of the system should not be compromised at all.

During manufacturing, the tolerances of all the components should be checked. These include how the following components fit together:

- Stator to the stator housing
- Bearings to the end housings and support plate
- Rotor shaft to the planetary gear
- Support plate to the stator housing
- Support plate to the drive-end housing
- Non-drive end housing to the stator housing

The fit is crucial to ensure the rotation of the bearings and so the rotor will not be out of balance. The fit can be checked and tested multiple times during the process to provide the ideal fit. Some components will require interference fits, and some will require a tight clearance fit for disassembly. A transition fit may be the best choice for the end housings.

The planetary gear used in the system is not specifically designed for speeds up to 18,000 rpm. It is designed for an automatic transmission, and most car engines do not exceed 7,000 rpm. Assuming a small safety factor, 10,000 rpm should not be a problem for the current gearset. Ideally, a gearset meant for higher speeds would be used. However, it proved difficult to find a gearset that could reach these speeds with the desired torque and reduction ratios. It is possible that one could be designed specifically for the needs of this project, and would be a great opportunity for another thesis.

Another important aspect to study is the vibrations in the frame. With sufficient tolerances, the system should minimize vibrations and losses. Currently, only a solid rotor has been analyzed for vibrations and natural frequencies. A more sophisticated design with a squirrel cage could be modeled and analyzed. The better the design, the more efficient the prototype will be, and the more magnetic flux can be induced into the rotor. The current rotor design should be tested for symmetry and balancing after it is made. If improperly balanced during the manufacturing process, the rotor will cause excessive vibrations therefore harming the bearings and possibly more components.

Since the electrical sheets are available from the stator lamination cuts, a laminated squirrel cage rotor should be considered. This design will typically provide the most electromagnetic benefits while reducing the losses. The design is much more complex than a solid rotor. The

strength of the rotor can also be of concern, as rotating hundreds of these steel sheets at high speeds could be difficult to balance, potentially leading to catastrophic failure.

Oil cooling has a large influence on the design of this system. Proper design of the cooling has not been analyzed. Computational fluid dynamics of the oil flow and airflow can be done to investigate the cooling properties of the system. However, this may not be necessary for initial testing. The prototype can be made with the current oil cooling design. A proper oil pump, fittings and cooling lines need to be obtained. This is easy to implement after the system is assembled. Measuring the temperature of the stator can be analyzed with the thermocouple, this will provide information if the motor is running too hot. Additional oil cooling lines and holes can be implemented without too much difficulty. If needed, extra holes can be drilled into the stator for the oil to pass through. The amount of oil flow needed can be tested by adjusting the flow rate on the pump. The amount of oil entering the system should be the same amount of oil draining from the system. This will provide a constant oil level. A rising oil level is of concern, because if the oil level rises and hits the rotor, it will inhibit the speed of the rotor and cause extra losses. A heat exchanger or something similar will cool the exiting oil before re-entering the system. This will require airflow through the heat exchanger, easily accessible at a proper test bench with a fan. Cooling ducts can also be added on the outside of the frame as shown in [30].

The design used to send oil to the planetary gear should be verified with real world testing. The bearing in the non-drive end housing needs to be sealed properly so the oil will flow from the input fitting into the hole in the rotor shaft. Sealing the bearing in the drive-end housing might also be required. The bearing glue will help with this however, *SKF* makes bearing seals that could be utilized as well. The planetary gear might require more oil flow than the stator oil cooling channels. The oil cooling channels design might have to change slightly if the end windings in the stator are larger than expected, as the ring on the non-drive end leaves some space for the end windings, but it is unknown exactly how much will be needed until the stator is made. The ring can be seen in Figure 22.

With the proper design of the oil cooling, thermal analysis of the entire machine can be done. Again, computational fluid dynamics can be used, or this can be tested in the real life. Real life testing may be easier, and if the system is not ran at full speed then the thermals are not of great concern. Multiple thermocouples will provide temperature verification. The efficiency can be measured once the motor is running by comparing the power input versus the power output.

Close to a hundred simulations were completed for this project. The design process for induction motors is iterative. This means that a lot more time could be spent adapting small changes into the design for benefits. The windings, electromagnetics and voltages could all be analyzed further to minimize losses, and improve the overall performance. Little geometry changes to the stator slots, air gap and stator slot openings can have a great influence on the machine. However, this is almost a never-ending process. The goal was to provide a good design with satisfactory characteristics. Incorporating small changes will sometimes only provide marginally better results and may not be worth the additional time required.

An interesting future development idea is to use 3D printing or additive manufacturing for the electric motor materials such as the stator and rotor. The stator would be the best initial

choice, as it does not rotate and incur many stresses. Printing methods such as selective laser sintering, or stereolithography are commonly used to print metals. These methods can provide material densities similar to the more common materials used for electric motors [43]. The thermal properties and electromagnetic properties of the metal used can be analyzed for this concept. In addition, as the material is fused together by a laser, so the mechanical and structural properties should be tested, especially if used for the rotor.

The bearings used are designed specifically for electric motors. The bearings are made from ceramic to provide resistance to eddy currents and magnetic induction [33]. Steel bearings are generally more susceptible to magnetic induction. Steel bearings could be tested to compare the difference. The ceramic bearings are more expensive and may not even be needed for this prototype, but are used to reduce any unnecessary losses.

In addition to the cost of the bearings, the cost of other components can be considered. The cost for the initial prototype is not of the greatest concern. In the future, reducing the amount of material used, the type of materials used, and the companies for producing the stator can be evaluated for areas of cost savings.

The overall efficiency and performance of the entire system is a key factor. Some items may need to be sacrificed on to improve others. As long as the final design works, is cost effective and efficient then the concept can be proved. Providing the required specifications to be competitive is probably the most important aspect to consider. If the design has benefits over other products on the market, then there is a place for this in the transportation industry, or possibly even other industries.

To summarize, below is a list of final items that need to be finished before the motor should be ordered:

- Voltage simulations
    - Fix convergence issues
    - Check voltage, current and torque levels
- Double layer winding definitions should be checked
- End winding parameters should be checked
- Correct BH curve used in the simulations
- Reduces the overall losses (Correct BH curve and simulation coefficients)

This is a list of items that should be done after the motor is ordered and during manufacturing:

- Tolerances should be checked
- Proper oil cooling design
- Verify converter will work

6 Conclusion

The objective of this thesis was to develop a final design for prototyping a high-speed induction motor with an integrated planetary gear. Many iterations of the design were completed to deliver a great foundation for manufacturing, proof of concept, and testing. The design was completed using FEM simulations and 3D modeling. Each iteration of the design and was analyzed in detail.

The project goal is to develop a compact and cost efficient electric drive solution for the transportation industry. The basic operating principals of an induction motor and the integration with a planetary gear were explained in detail. This concept is compared to similar systems that use electric motors in conjunction with a planetary gear.

Starting with previous designs, the mechanical design was further developed with the use of Creo Parametric modeling software. This includes the most important design features and things to consider when making a prototype of an induction motor. The method to integrate the induction motor and planetary gear is also explained. Items such as thermals, cost and manufacturability were covered.

To aid in the demanding process of designing an induction motor, FEM Simulations with Elmer were used. This extensive process required close to a hundred simulations of different types to determine a final design. The geometry of the stator slots, magnetic flux densities, currents, voltages, torque levels and losses were put into extreme scrutiny. Paraview and Matlab provided a visual representation of what each change to the design did, and how it affected the motor specifications.

Many other parts of this design can be researched in more detail in the future. Designing an induction motor with an integrated planetary gear is a challenging task. Much more time could be spent developing this design and concept. However, the most important task should be to test the proof of concept. Every change made can affect other aspects of the prototype and the final operating principals. A different planetary gear may be required for high-speed tests of above 10,000 rpm. A few small items need to be finalized, and then the design is at a stage where the next step is to order and manufacture the components.

References

[1] J. Puranen, "Induction motor versus permanent magnet synchronous motor in motion control applications: A comparative study," Lappeenranta University of Technology, Lappeenranta, 2006.

[2] T. Jokinen, "High-speed electrical machines, Conference on high speed technology," Lappeenranta, 1988.

[3] N. Hashemnia and B. Asaei, "Comparative Study of Using Different Electric Motors in the Electric Vehicles," in *International Conference on Electrical Machines*, Tehran, 2008.

[4] J. Pyrhönen, T. Jokinen and V. Hrabovcov´a, Design of Rotating Electrical Machines, John Wiley & Sons, Ltd, 2008.

[5] U. Nikita, "High-Speed Soild-Rotor Induction Machine - Calculation Program," Lappeenranta University of Technology, Lappeenranta, 2012.

[6] K. Yamazaki, A. Suzuki, M. Ohto and T. Takaura, "Harmonic Loss and Torque Analysis of High-Speed Induction Motors," IEEE Transactions on Industry Applications, 2012.

[7] J. Mäntylä, "Design of a high-speed propulsion motor," Aalto University, Espoo, 2016.

[8] J. Huppunen, "High-speed solid-rotor induction machine - Electromagnetic calculation and design," Lappeenranta University of Technology, Lappeenranta, 2004.

[9] Y. Asano, Y. Honda, H. Mukakami, Y. Takeda and S. Morimoto, "Novel Noise Improvement Technique for a PMSM with Concentrated Winding," Matsushita Electric Industrial Co., Ltd., Osaka, 2002.

[10] "Single-tooth motors could bite into the EV market," Drives & Controls, 09 July 2013. [Online]. Available: http://drivesncontrols.com/news/fullstory.php/aid/4009/Single-tooth_motors_could_bite_into_the_EV_market.html?current_page=NO_PAGE. [Accessed March 2017].

[11] M. Hadžiselimović, T. Marčič, B. Štumberger and I. Zagradišnik, "Winding type influence on efficiency of an induction motor," University of Maribor, Faculty of Energy Technology, Maribor, 2001.

[12] M. E. Dale and C. R. Sullivan, "Comparison of Single-Layer and Multi-Layer Windings with Physical Constraints or Strong Harmonics," IEEE, Montreal, 2006.

[13] "Types of Armature Windings Part1," Your Electrical Home, 14 February 2012. [Online]. Available: http://www.yourelectrichome.com/2012/02/types-of-armature-windings.html. [Accessed March 2017].

[14] "Difference Between Star and Delta Connection," Circuit Globe, [Online]. Available: http://circuitglobe.com/difference-between-star-and-delta-connection.html. [Accessed March 2017].

[15] "Delta or Star connection of machine windings?," Emetor, 26 June 2013. [Online]. Available: https://www.emetor.com/blog/post/delta-or-star-connection-machine-windings/. [Accessed April 2017].

[16] M. Popescu, D. Staton, A. Boglietti, A. Cavagnino, D. Hawkins and J. Goss, "Modern Heat Extraction Systems for Electrical Machines – A Review," IEEE.

[17] J. Lähteenmäki, "Design and Voltage Supply of High-Speed Induction Machines," Helsinki University of Technology, Espoo, 2002.

[18] D. Gerada, A. Mebarki, N. Brown, K. Bradley and C. Gerada, "Design Aspects of High-Speed High-Power-Density Laminated-Rotor Induction Machines," *IEEE Transactions on Industrial Electronics,* vol. 58, pp. 4039-4047, 2011.

[19] D. Gerada, A. Mebarki, N. Brown, C. Gerada, A. Cavagnino and A. Boglietti, "High-Speed Electrical Machines: Technologies, Trends and Developments," *IEEE Transactions on Instrial Electronics,* vol. 61, pp. 2946-2959, 2014.

[20] "Planetary Gear Sets - Opeartion and Theory," Engrade, [Online]. Available: https://wikis.engrade.com/planetarygearsetsoperati. [Accessed February 2017].

[21] K. Tammi, "Compact and cost-efficient drive solutions for electrical vehicle applications," Aalto University, Espoo, 2016.

[22] M. Ehsani, Y. Gao and J. M. Miller, "Hybrid Electric Vehicles: Architecture and Motor Drives," Invited Paper, 2007.

[23] A. Mylläri, "High Speed Electric Motor in Diesel-Electric Hybrid Mobile Machinery," Aalto University, Espoo, 2012.

[24] K. Rajashekara, "History of Electric Vehicles in General Motors," *IEEE Transactions on Industry Applications,* vol. 30, pp. 897-904, 1994.

[25] L. Brooke, "Inside the Bolt EV," Automotive Engineering, 2017.

[26] C. Ruoff, "Charged Electric Vehicles Magazine," 6 January 2016. [Online]. Available: https://chargedevs.com/features/qa-with-teslas-lead-motor-engineer-full-interview/. [Accessed April 2017].

[27] A. S. Rodríguez, "Dynamic Behavior of high-speed rotor," Aalto University, Espoo, 2017.

[28] H.-C. Lahne and D. Gerling, "Comparision of State-of-the-Art High-Speed High-Power Machines," Universistaet der Bundeswehr Muenchen, Neubiberg, 2015.

[29] D. Ahmet, M. Onur and D. Tunc, "A Performance Comparison of Different Rotor Types for High-Speed Induction," Istanbul.

[30] Y. G. Mekuria, "Development of a High Speed Solid Rotor Asynchronous Drive fed by a Frequency Converter System," Technischen Universität Darmstadt, Darmstadt, 2013.

[31] M. Centner, R. Hanitsch and U. Schäfer, "Comparison of high-speed induction motors employing cobalt-iron and silicon electrical steel," in *International Conference on Electrical Machines*, Berlin, 2008.

[32] T. R. Kuphaldt, "Lessons In Electric Circuits -- Volume II," 2010. [Online]. Available: http://www.malayalam.net/howto/LessonsInElectricCircuits/AC/AC_13.html. [Accessed January 2017].

[33] SKF, "SKF hybrid bearings for high speed electric motors," [Online]. Available: http://www.skf.com/group/industry-solutions/home-appliances/requirements/low-noise/skf-hybrid-bearings-for-high-speed-electric-motors/index.html. [Accessed February 2017].

[34] ABB, *ABB machinery drives - ACS850 0.5 to 700 hp/0.37 to 560 kW,* 2014.

[35] R. Deshmukh, A. J. Moses and F. Anayi, "Behavior of three-phase induction motors with variable stator coil winding," Wolfson Centre for Magnetics Technology, Cardiff University, Cardiff, 2006.

[36] Z. I. Inc, *ZF 5HP18 Automatic Transmission - Spare Part Catalog,* 2003.

[37] J. Ruokolainen, M. Malinen, P. Råback, T. Zwinger, A. Pursula and M. Byckling, *ElmerSolver Manual,* CSC - IT Center for Science, 2016.

[38] P. Råback, M. Malinen, J. Ruokolainen, A. Pursula and T. Zwinger, *Elmer Models Manual,* CSC - IT Center for Science, 2016.

[39] P. Ponomarev, *FEM Modeling of PMSWs Using Elmer,* Lappeenranta University of Technology, 2014.

[40] S. Kwon, J. Lee, B. Lee, J. Kim, K. Ha and J. Hong, "Loss Distribution of Three-Phase Induction Motor and BLDC Motor According to Core Materials and Operating," IEEE Transactions of Magnetics, Seoul, 2009.

[41] J. Saari, "Thermal Analysis of High-speed Induction Machines," Acta Polytechnica Scandinavica, Espoo, 1998.

[42] R. Sundaria, "3-D Eddy Current Modelling of Laminations to Study Edge Effects," Aalto University, Espoo, 2016.

[43] M. Garibaldi, "Can we "3D-Print" and Electric Motor?," University of Nottingham, Nottingham, 2015.

Appendices

Appendix 1: Transmission Disassembly Figures. 4 Pages.
Appendix 2: Example SIF file. 9 Pages.
Appendix 3: Stator Drawing File. 1 Page.

Appendix 1: Transmission Disassembly Figures

Donated automatic transmission

Transmission oil pan - first step for disassembly

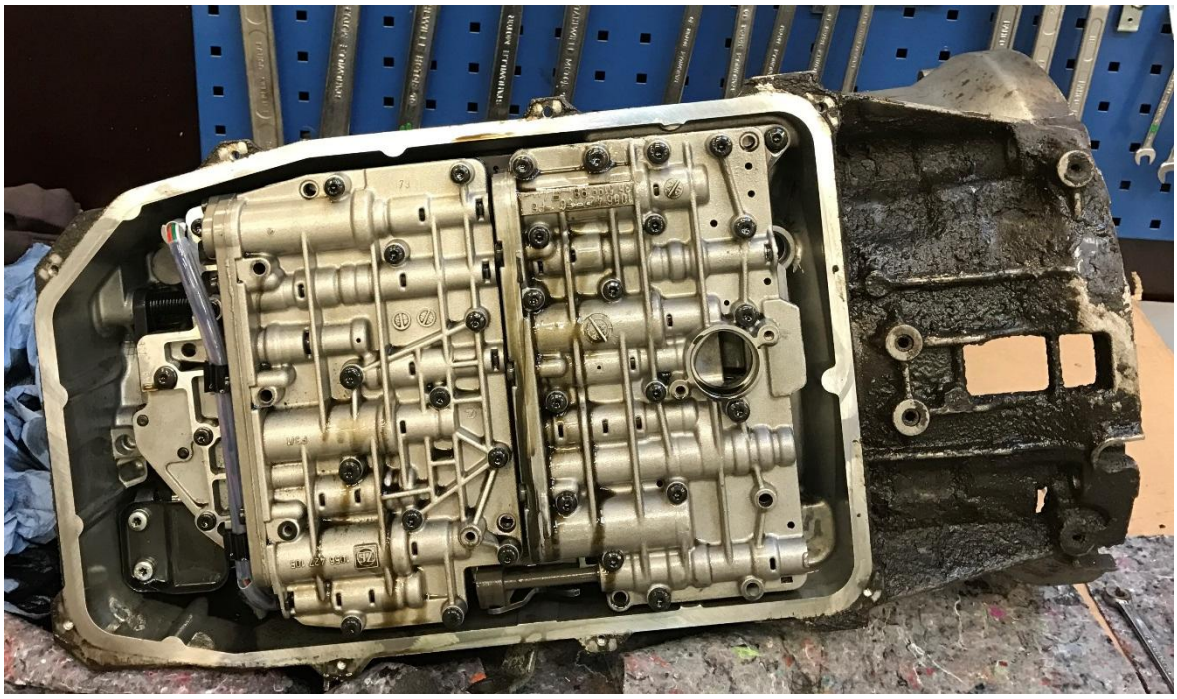

Transmission valve train

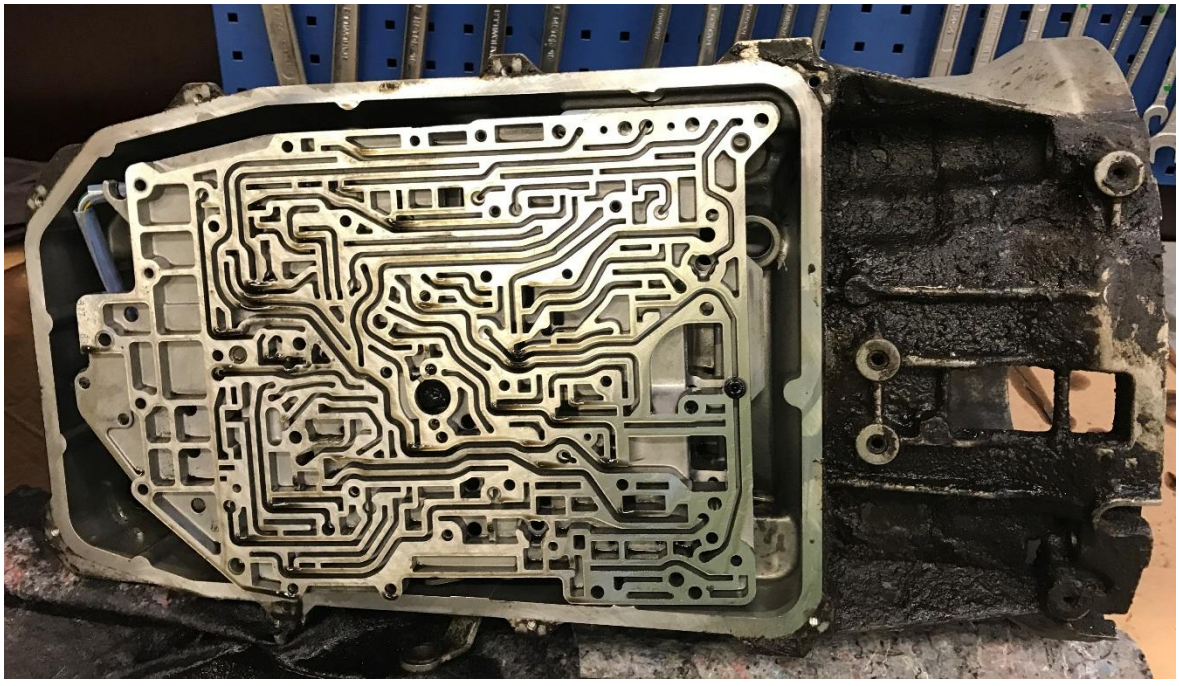

Transmission valve train channels

Transmission input shaft

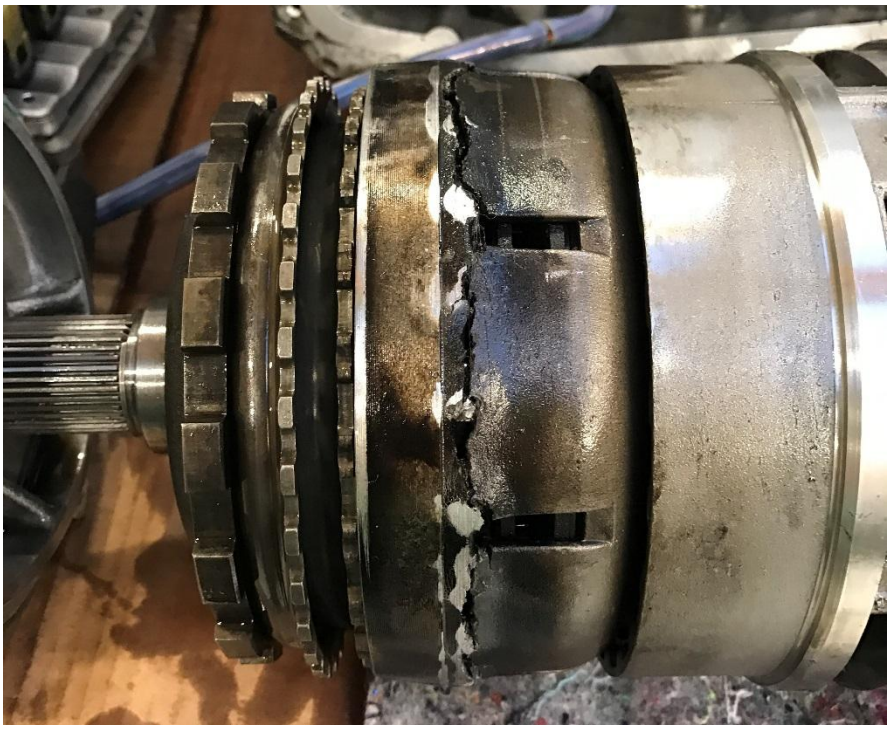

Broken component - clutch pack housing

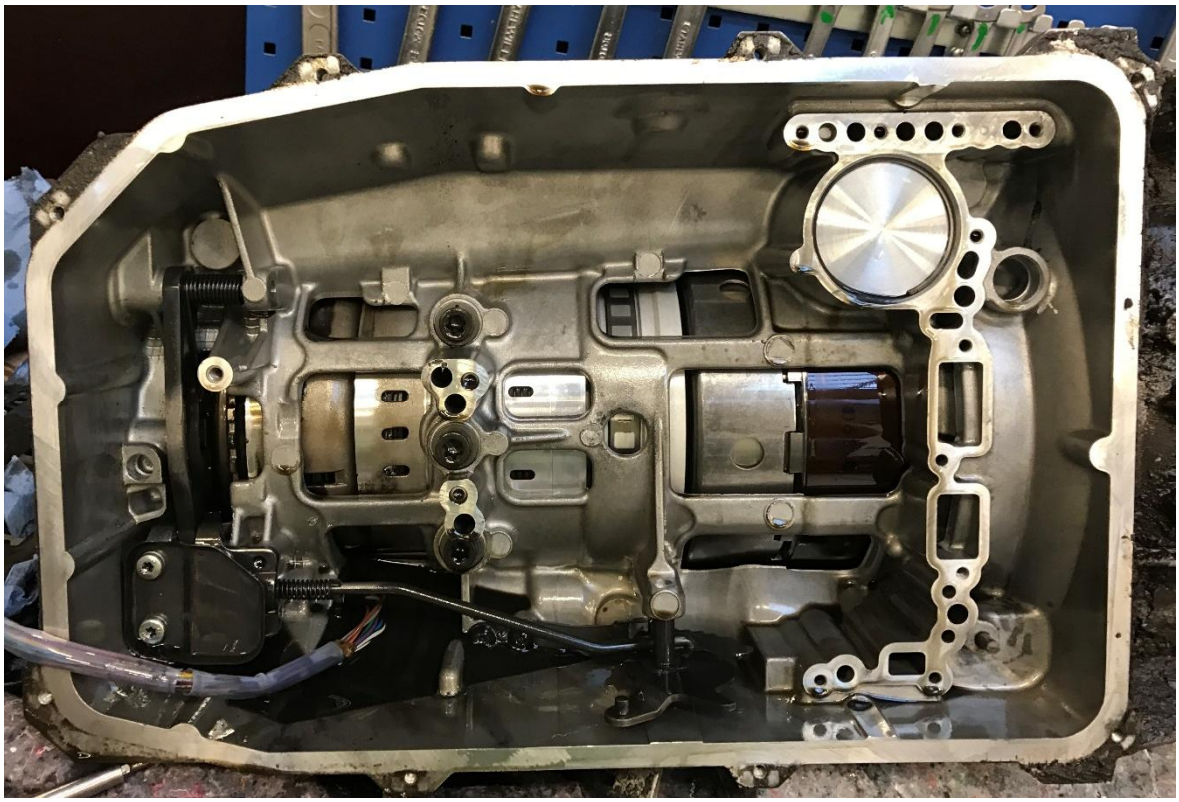

Transmission inside – large bolts to remove clutch packs

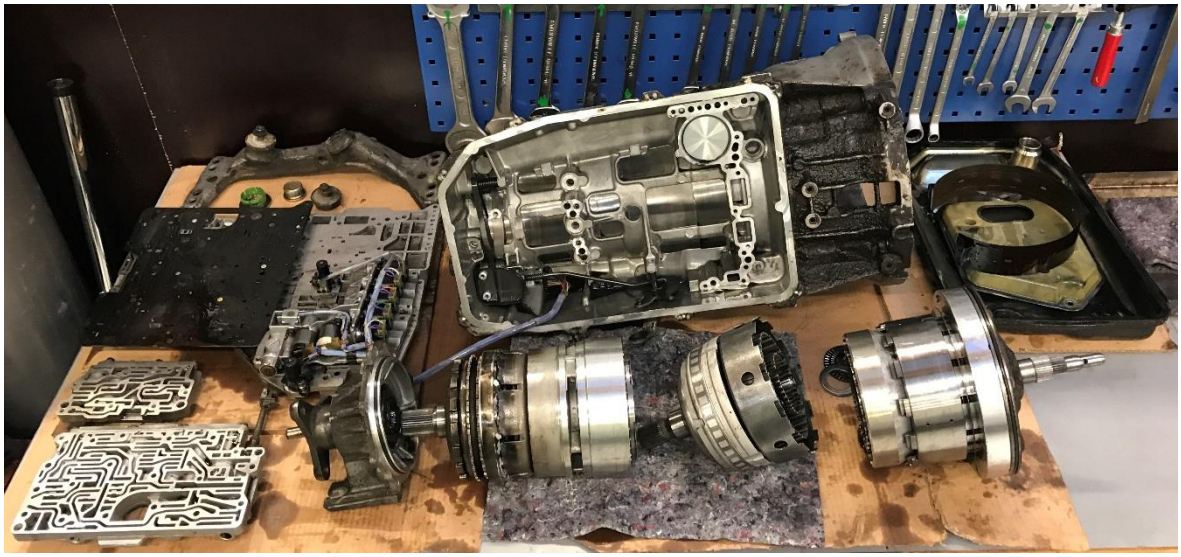

Entire disassembled transmission. Input from right to left

Appendix 2: Example SIF file

```
!Made for Master's Thesis of Jesse Mäntylä, Aalto University, Department of Mechanical Engineering 05/2016
!Modified by Kevin Campbell 05/2017

$ w_mech_rpm = 18000 ![rpm] Synchronous rotation speed
$ w_mech = w_mech_rpm*2*pi/60 ![rad/s] Synchronous angular velocity
$ pp = 2 !Pole pairs
$ w_elec = w_mech*pp ![rad/s] Electrical angular velocity
$ r_inner = 0.075 ![m] Rotor radius
$ r_outer = 0.0785 ![m] Rotor radius with air gap
$ J_stator = 4.53e6 !Current density in the slot
$ L_rot = 0.08 !Length of the motor
$ area_bar = 0.000047
$ SLIP = 0.98 !Rotor slip
$ Imom  = 0.03 !Moment of Inertia of the rotor
$ InitialSpeed = w_mech*SLIP !Tnitial rotor speed [rad/s]
$ InitialAngle = 0 !Initial rotor angle [rad]

!Circuit module, cage windings
$ R_b2b = 0.000016 ![Ohm] bar-2-bar end ring rotor resistance
$ L_b2b = 0.000000007 ![H] bar-2-bar end ring rotor inductance

$ Circuits = 1
$ results1 = "results_9"

!!!!!!HEADER!!!!!!
Header
 CHECK KEYWORDS Warn
 Mesh DB "." "Angled_9"
 Include Path "bar_sections"
 Results Directory ""
End

Simulation
 Max Output Level = 3 !Message level max. 10.

 Coordinate System = Cartesian 2D
 Coordinate Mapping(3) = 1 2 3
 Coordinate Scaling= 0.001

 Simulation Type = Transient
 Steady State Max Iterations = 1
 Output Intervals = 1
 Timestepping Method = BDF
 BDF Order = 1
 Timestep Sizes =$ 1/(w_elec/2/pi)/90
 Timestep Intervals = 8000
```

```
 imom  = Real $Imom
 Circuit Model Depth = Real $ L_rot

 loadtorque1 = Real 375
 loadtorqueAngle1 = Real 30
 loadtorque2 = Real 375
 loadtorqueAngle2 = Real 70
 loadtorque3 = Real 375
 loadtorqueAngle3 = Real 80
 loadtorque4 = Real 375
 loadtorqueAngle4 = Real 90
End

!!!!!!SOLVERS!!!!!!
!Mesh deforming
Solver 1
 Equation = Motion
 Procedure = "FreeMotion" "FreeMotion"
 Exec Solver = Always !Before Timestep
End

Solver 2
 Equation = MeshDeform2
 Procedure = "RigidMeshMapper" "RigidMeshMapper"
 Exec Solver = Before Timestep
End

!Cirquit equations
Solver 3
 Equation = Circuits
 Variable = X
 Procedure = "CircuitsAndDynamics" "CircuitsAndDynamics"! "Circuits2D"
"CircuitsAndDynamics"
 Exec Solver = Always
End

!Magnetic vector potential A
Solver 4
 Equation = MgDyn2D
 Procedure = "MagnetoDynamics2D" "MagnetoDynamics2D"
 Exec Solver = Always
 Variable = A
 Apply Mortar BCs = Logical True

 Steady State Convergence Tolerance = 1e-05

 Nonlinear System Convergence Tolerance = 1e-5
 Nonlinear System Max Iterations = 40
```

```
 Nonlinear System Min Iterations = 1
 Nonlinear System Relaxation Factor = 1.0
 Nonlinear System Newton After Iterations = 3

 Newton-Raphson Iteration = Logical True
 Export Lagrange Multiplier = Logical True

 Linear System Normalize Guess = Logical True
 Linear System Abort Not Converged = True
 Linear System Solver = Iterative
 Linear System Iterative Method = GCR
 Linear System GCR Restart = 1000
 Bicgstabl Polynomial Degree = 4
 Linear System Preconditioning = Ilu2
 Linear System Max Iterations = 1500
 Linear System Residual Output = Integer 10
 Linear System Convergence Tolerance = 2.0e-10 ! 2.0e-6
End

!Other fields from potential A, automatically flux density B [T]
Solver 5
 Equation = MagDynCalc
 Procedure = "MagnetoDynamics" "MagnetoDynamicsCalcFields"
 Potential Variable = "A"
 Exec Solver = Always ! After Timestep

 Calculate Current Density = Logical True
 Calculate Electric Field = Logical True
 Calculate Magnetic Field Strength = Logical True
 Calculate Magnetic Vector Potential = Logical True

!GNF Torque calculation, a new feature
 Calculate Nodal Forces = Logical True
 Calculate Magnetic Torque = Logical True

!Iterative
 Linear System Solver = "Iterative"
 Linear System Preconditioning = ILU2
 Linear System Residual Output = 10
 Linear System Max Iterations = 100
 Linear System Iterative Method = BicgstabL
 Linear System Convergence Tolerance = 1.0e-8
 Linear System Symmetric = True
End

Solver 6
 Exec Solver = Always
 Equation = CircOutput
 Procedure = "CircuitsAndDynamics" "CircuitsOutput"
```

```
End

!VTU Format
Solver 7
 Exec Solver = After Simulation! After Timestep
 Equation = ResultOutput
 Procedure = "ResultOutputSolve" "ResultOutputSolver"
 Vtu Format = True
 Output Directory = $ results1
 Single Precision = True!Default = false
 Save Geometry Ids = True
End

!Save scalars
Solver 8
 Exec Solver = After Timestep
 Output Directory = $ results1
 Filename = scalars.dat
 Procedure = "SaveData" "SaveScalars"
End

Solver 9
 Equation = "Fourier"
 Exec Solver = Before Saving
 Procedure = "FourierLoss" "FourierLossSolver"
 Target Variable = "A"

 Fourier Start Cycles = Integer 1
 Fourier Integrate Cycles = Integer 6
 !k - number of harmonic components calculated, must be high enough to capture slotting
effect
 Fourier Series Components = Integer 12

 Frequency = Real 600.0

 Fourier Loss Filename = File "Loss.dat"
 Harmonic Loss Linear Exponent = Real 1.7      !b1
 Harmonic Loss Quadratic Exponent = Real 2.0   !b2

 Linear System Symmetric = True
 Linear System Solver = "Iterative"
 Linear System Residual Output = 100
 Linear System Max Iterations = 5000
 Linear System Iterative Method = GCR
 Linear System Convergence Tolerance = 1.0e-4
End

!!!!!!EQUATIONS!!!!!!
Equation 1
```

```
        Active Solvers(3) = 3 4 5
End

Equation 2
        Active Solvers(4) = 3 4 5 9
End

!!!!!!INITIAL CONDITIONS, CIRCUIT MODEL!!!!!!
Initial Condition 1
  Rotor Velo = Real $InitialSpeed
End

Initial Condition 2
  Rotor Angle = Real $InitialAngle
End

!!!!!!BOUNDARY CONDITIONS!!!!!!
Boundary Condition 1
 Name = "BC_outer"
 Target Boundaries(1) = 2
 A = Real 0
End

!Mortar
Boundary Condition 2
 Name = "BC_rotation"
 Target Boundaries(1) = 1
 Discontinuous Boundary = Logical True
 Mortar BC = Integer 4
 Anti Rotational Projector = Logical True
 Galerkin Projector = Logical True
End

!!!!!!BODY FORCES!!!!!!
!Rotation of the rotor

Body Force 1
 Name = "Rotation"
 Mesh Rotate 3 = Variable Rotor Angle
 Real MATC "360*tx(0)/(2*pi)"
End

Body Force 2
 Name = "Current_U1"
 Current Density = Variable Time
 Real MATC "J_stator*sin(w_elec*tx(0)+(2*pi)*0)"
End

Body Force 3
```

```
 Name = "Current_U2"
 Current Density = Variable Time
 Real MATC "-J_stator*sin(w_elec*tx(0)+(2*pi)*0)"
End

Body Force 4
 Name = "Current_V1"
 Current Density = Variable Time
 Real MATC "J_stator*sin(w_elec*tx(0)+(2*pi)/3)"
End

Body Force 5
 Name = "Current_V2"
 Current Density = Variable Time
 Real MATC "-J_stator*sin(w_elec*tx(0)+(2*pi)/3)"
End

Body Force 6
 Name = "Current_W1"
 Current Density = Variable Time
 Real MATC "J_stator*sin(w_elec*tx(0)-(2*pi)/3)"
End

Body Force 7
 Name = "Current_W2"
 Current Density = Variable Time
 Real MATC "-J_stator*sin(w_elec*tx(0)-(2*pi)/3)"
End

!!!!!!BODIES!!!!!!
Body 1
 Name = "U1"
 Target Bodies(1) = 5
 Equation = 1
 Material =1
 Body Force =2
End

Body 2
 Name = "U2"
 Target Bodies(1) = 8
 Equation = 1
 Material =1
 Body Force =3
End

Body 3
 Name = "V1"
 Target Bodies(1) = 9
```

```
 Equation = 1
 Material =1
 Body Force =4
End

Body 4
 Name = "V2"
 Target Bodies(1) = 6
 Equation = 1
 Material =1
 Body Force =5
End

Body 5
 Name = "W1"
 Target Bodies(1) = 7
 Equation = 1
 Material =1
 Body Force =6
End

Body 6
 Name = "W2"
 Target Bodies(1) = 10
 Equation = 1
 Material =1
 Body Force =7
End

Body 7
 Name = "Stator"
 Target Bodies(1) = 2
 Equation = 2
 Material = 2
End

Body 8
 Name = "Rotor"
 Target Bodies(1) = 12
 Equation = 2
 Material = 2
 Body Force = 1
 Torque Groups(1) = Integer 1
End

Body 9
 Name = "Stator_air_gap"
 Target Bodies(1) = 4
 Equation = 1
```

```
 Material = 1
End

Body 10
 Name = "Rotor_air_gap"
 Target Bodies(1) = 11
 Equation = 1
 Material = 1
 Body Force = 1
 r outer = Real $ r_outer
 r inner = Real $ r_inner
End

Body 11
 Name = "Wedge"
 Target Bodies(1) = 3
 Equation = 1
 Material = 3
End

Body 12
 Name = "Shaft"
 Target Bodies(1) = 1
 Equation = 1
 Material = 1
 Body Force = 1
 Torque Groups(1) = Integer 1
End

Include "cage_body30"

!!!!!!!Components!!!!!!
include "cage.definitions.30"


!!!!!!MATERIALS!!!!!!
Material 1
 Name = "Air"
 Relative Permeability = 1
 Relative Permittivity = 1
 Electric Conductivity = 0
End

Material 2
Name = "Iron"
 Include el_steel_M400_50A
 Relative Permittivity = Real 1

 !C1
```

```
 Harmonic Loss Linear Coefficient = Variable "Frequency"
 Real
   0.0 250.0
   10000.0 250.0
End

 !C2
 Harmonic Loss Quadratic Coefficient = Variable "Frequency"
 Real
   0.0 0.8
   10000.0 0.8
 End
End


Material 3
Name= "Wedge"
 Relative Permeability = 1
 Relative Permittivity = 1
End

Material 4
 Name = "Copper"
 Relative Permeability = 1
 Electric Conductivity = 59.59e6  ![S/m]
 Relative Permittivity = 1
End
```

Appendix 3: Stator Drawing File

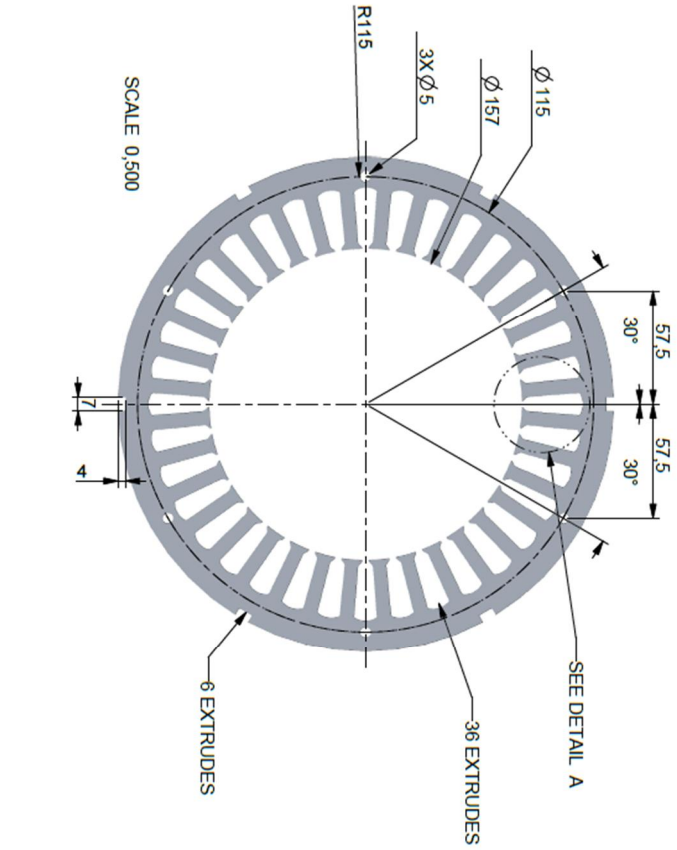

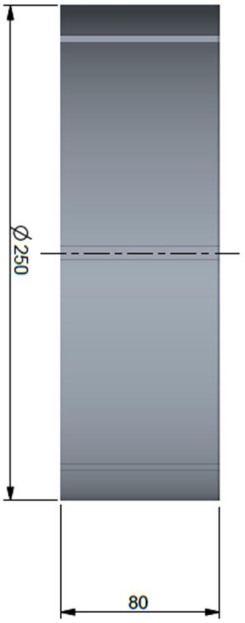

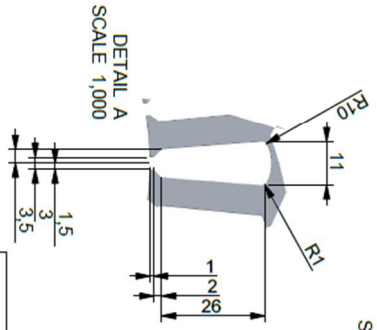

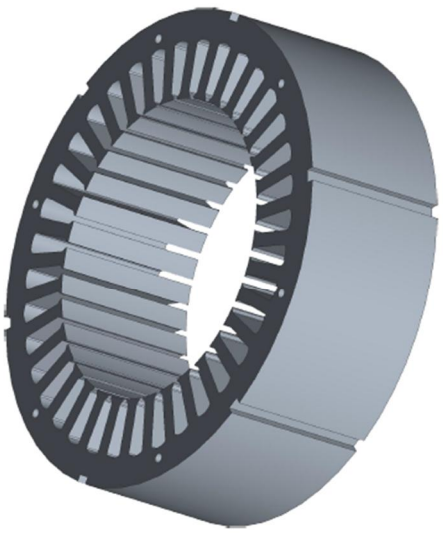

Aalto University	
TITLE	Induction Motor Stator
SIZE	A3
Date	15.4.2017
Drawing By	Kevin Campbell
REV	1
SCALE: 0.500	All dimensions in mm
SHEET 1 OF 1	